AGU PUBLICATIONS

Journal of Advances in Modeling Earth Systems

RESEARCH ARTICLE

10.1002/2014MS000315

**Key Points:**
- Most variances in cloud fields can be explained by a small number of parameters
- Results for stratocumulus are sensitive to vertical resolution
- Critical parameters in shallow cumulus are related to vertical velocity skewness

**Correspondence to:**
M. Wang,
Minghuai.Wang@pnnl.gov or Z. Guo,
Zhun.Guo@pnnl.gov

**Citation:**
Guo, Z., M. Wang, Y. Qian, V. E. Larson, S. Ghan, M. Ovchinnikov, P. A. Bogenschutz, C. Zhao, G. Lin, and T. Zhou (2014), A sensitivity analysis of cloud properties to CLUBB parameters in the single-column Community Atmosphere Model (SCAM5), *J. Adv. Model. Earth Syst.*, *06*, doi:10.1002/2014MS000315.

Received 5 MAR 2014
Accepted 2 JUL 2014
Accepted article online 8 JUL 2014

This is an open access article under the terms of the Creative Commons Attribution-NonCommercial-NoDerivs License, which permits use and distribution in any medium, provided the original work is properly cited, the use is non-commercial and no modifications or adaptations are made.

# A sensitivity analysis of cloud properties to CLUBB parameters in the single-column Community Atmosphere Model (SCAM5)

**Zhun Guo[1,2], Minghuai Wang[1], Yun Qian[1], Vincent E. Larson[3], Steven Ghan[1], Mikhail Ovchinnikov[1], Peter A. Bogenschutz[4], Chun Zhao[1], Guang Lin[1], and Tianjun Zhou[2]**

[1]Pacific Northwest National Laboratory, Richland, Washington, USA, ~~[2]Institute of Atmospheric Physics, Beijing, China,~~ [3]University of Wisconsin–Milwaukee, Milwaukee, Wisconsin, USA, [4]National Center for Atmospheric Research, Boulder, Colorado, USA

**Abstract** In this study, we investigate the sensitivity of simulated shallow cumulus and stratocumulus to selected tunable parameters of Cloud Layers Unified by Binormals (CLUBB) in the single-column version of Community Atmosphere Model version 5 (SCAM5). A quasi-Monte Carlo (QMC) sampling approach is adopted to effectively explore the high-dimensional parameter space and a generalized linear model is adopted to study the responses of simulated cloud fields to tunable parameters. One stratocumulus and two shallow cumulus cases are configured at both coarse and fine vertical resolutions in this study. Our results show that most of the variance in simulated cloud fields can be explained by a small number of tunable parameters. The parameters related to Newtonian and buoyancy-damping terms of total water flux are found to be the most influential parameters for stratocumulus. For shallow cumulus, the most influential parameters are those related to skewness of vertical velocity, reflecting the strong coupling between cloud properties and dynamics in this regime. The influential parameters in the stratocumulus case are sensitive to the vertical resolution while little sensitivity is found for the shallow cumulus cases, as eddy mixing length (or dissipation time scale) plays a more important role and depends more strongly on the vertical resolution in stratocumulus than in shallow convections. The influential parameters remain almost unchanged when the number of tunable parameters increases from 16 to 35. This study improves understanding of the CLUBB behavior associated with parameter uncertainties and provides valuable insights for other high-order turbulence closure schemes.

Author Proof

## 1. Introduction

Clouds play a critical role in regulating the Earth's hydrological and energy cycles and contribute to the large uncertainty in climate modeling [e.g., *Bony and Dufresne*, 2005]. It is therefore critical to understand clouds and to accurately simulate them in global climate models.

Stratiform clouds and shallow cumulus are treated by separate and independent parameterizations in most general circulation models (GCMs), due to challenges in representing them in a single framework. However, this can produce unrealistic results when these two cloud types interact with each other [*Arakawa*, 2004], as, for example, in the stratocumulus-cumulus transition regime, where stratocumulus often breaks up into cumulus layers with much lower albedo and shortwave cloud radiative forcing. In addition, using separate cloud parameterizations makes it challenging to couple them with the same set of cloud microphysics.

An incomplete third-order turbulence closure parameterization coupled with assumed probability density functions (PDFs), named Cloud Layers Unified by Binormals (CLUBB), offers an opportunity to avoid such problems [*Golaz et al.*, 2002a, 2002b; *Larson et al.*, 2002; *Larson and Golaz*, 2005; http://clubb.larson-group.com]. CLUBB predicts subgrid variations and high-order moments of total water, liquid potential temperature, and vertical velocity. Based on these predicted variations and high-order moments, a particular PDF member is selected from the assumed double Gaussian PDF family. The double Gaussian PDF is capable of representing vertical velocity skewness and other nonzero third-order moment and has been shown to perform better than the single Gaussian or double delta function PDFs [*Larson et al.*, 2002]. This allows CLUBB to serve as a unified parameterization to simulate both cumulus and stratocumulus clouds [*Larson et al.*, 2012].

 © 2014. The Authors. 

AGU Journal of Advances in Modeling Earth Systems 10.1002/2014MS000315

CLUBB has recently been implemented into the Community Atmosphere Model version 5 (CAM5) to provide a unified treatment for turbulence, stratiform cloud macrophysics, and shallow convection [*Bogenschutz et al.*, 2012, 2013]. The single-column version of CAM5 (SCAM5) with CLUBB simulates more realistic shallow convective clouds and transitional boundary layer clouds (i.e., cumulus under stratocumulus) and produces a more robust response in vertical and temporal resolution compared with the standard SCAM5 [*Bogenschutz et al.*, 2012]. Moreover, CLUBB significantly improves the performance of CAM5 in the simulation of the stratocumulus to trade wind cumulus transition in the subtropical oceans [*Bogenschutz et al.*, 2013]. CLUBB also leads to improvements in the single-column and global versions of the Geophysical Fluid Dynamics Laboratory Atmosphere Model version 3; for example, it improves the simulation skill in coastal stratocumulus, especially at higher horizontal resolution [*Guo et al.*, 2010, 2011, 2014]. AQ1

CLUBB, like many other parameterizations, includes multiple tunable parameters. The tunable parameters in CLUBB are partly related to the terms in the prognostic equations that are unclosed using the assumed PDF, such as pressure terms and eddy diffusivity terms, which are also common to many other high-order turbulence closure parameterization [e.g., *Cheng et al.*, 2005; *Lappen and Randall*, 2001]. Many of these parameters cannot be derived theoretically and the current values of some of these parameters in CLUBB are empirically determined [*Golaz et al.*, 2002a, ~~2002b~~]. *Golaz et al.* [2007] applied an ensemble-based calibration framework to a standalone version of CLUBB to optimize some parameters to best fit benchmark simulations. Further studies are needed to examine how sensitive model simulations are to these tunable CLUBB parameters. AQ2

Sensitivity analysis (SA) offers a way to efficiently answer these questions. It quantifies parametric sensitivities and helps to understand which processes contribute most to the parameterization outcome through an analysis of the statistical distribution of model outputs. Such a statistical output distribution is generated by sampling multiple possible parameter values across the multidimensional model parametric space. It is a more comprehensive approach when compared with "one-at-a-time" sensitivity tests that cannot take parameter interactions into account [*Saltelli and Annonia*, 2010].

SA has been applied to advancing climate modeling [e.g., *Zhao et al.*, 2013; *Ma et al.*, 2013]. For example, *Zhao et al.* [2013] investigated the sensitivity of net radiative fluxes at the top of atmosphere to 16 selected uncertain parameters related to cloud microphysics and aerosol processes and emissions in the CAM5 and found that the size threshold parameter related to autoconversion of cloud ice to snow is one of the most influential parameters. *Ma et al.* [2013] applied SA to quantify source-receptor relationships of black carbon simulations in CAM5.

Author Proof

A single-column model is a direct and computationally efficient method to investigate cloud parameterizations in response to the perturbations of parameters. Therefore, SCAM5 is applied to simulate two contrasting cloud types in this study. We adopt an SA framework that integrates an exploratory sampling approach (quasi-Monte Carlo), and a generalized linear model analysis, for SA of SCAM5 results. The goal of this study is to explore the sensitivity of model simulations to CLUBB tunable parameters and to identify the most influential parameters that may be targeted for further calibration and sensitivity studies in the future. This paper is organized as follows. Section 2 details the CLUBB, SCAM5, and the SA methodology. The SA of the SCAM5-simulated variation of cloud fraction associated with tunable parameter is presented in section 3. The findings are summarized and discussed in section 4.

## 2. Methodology

### 2.1. Brief Description Model and Parameterization

CLUBB is a higher-order turbulence closure based on an assumed triple-joint PDF of liquid water potential temperature ($\theta_l$), total water mixing ratio ($q_t$), and vertical velocity ($w$) [*Golaz et al.*, 2002a, 2002b]. CLUBB predicts grid-mean values ($\bar{\theta}_l$, $\bar{q}_t$, $\bar{w}$, horizontal winds $\bar{u}$ and $\bar{v}$), variances ($\overline{w'^2}$, $\overline{q_t'^2}$, $\overline{\theta_l'^2}$, $\overline{u'^2}$, $\overline{v'^2}$), scalar terms ($\overline{q_t'\theta_l'}$, $\overline{w'q_t'}$, $\overline{w'\theta_l'}$), and the third-order moment of vertical velocity $\overline{w'^3}$ [*Golaz et al.*, 2002a, ~~2002b~~; *Larson and Golaz*, 2005; *Larson et al.*, 2012]. Thirteen PDF parameters used to determine the triple-joint PDF are then derived based on 10 predictive moment equations related to $\theta_l$, $q_t$, and $w$, with some additional assumptions [*Larson et al.*, 2002]. These 13 PDF parameters include the weight of PDF (*mixt*), the width of each Gaussian along w, $q_t$, and $\theta_l$ coordinate ($\tilde{\sigma}_w$, $\tilde{\sigma}_{q_t1}$, $\tilde{\sigma}_{q_t2}$, $\tilde{\sigma}_{\theta_l1}$, $\tilde{\sigma}_{\theta_l2}$), the mean of each Gaussian ($\widehat{w_1}$, $\widehat{w_2}$, $\widetilde{\theta_{l1}}$, $\widetilde{\theta_{l2}}$, $\widetilde{q_{t1}}$, $\widetilde{q_{t2}}$), and an intra-Gaussian correlation between $q_t$ and $\theta_l$ ($r_{q_t\theta_l}$). The intra-Gaussian correlations

 © 2014. The Authors. 

AGU Journal of Advances in Modeling Earth Systems 10.1002/2014MS000315

between $q_t$, $\theta_l$ and $w$ ($r_{wq_t}$ and $r_{w\theta_l}$) are set to zero in CLUBB, and the widths of each Gaussian along $w$ ($\tilde{\sigma}_{w1}$, $\tilde{\sigma}_{w2}$) are equal, i.e., $\tilde{\sigma}_{w1}=\tilde{\sigma}_{w2}=\sigma_w\sqrt{\overline{w'^2}}$ [*Larson et al.*, 2002]. A particular triple-joint PDF, $P\ (\theta_l,\ q_t,\ w)$ is then selected from the double Gaussian mixture family by mapping those 13 PDF parameters. The double Gaussian PDF leads to a better performance in simulating the highly skewed PDFs observed in cumulus layers compared with the single Gaussian or double delta function PDFs [*Larson et al.*, 2002]. By integrating over the assumed triple-joint PDF, all high-order terms, which occur in the predictive equations of CLUBB including $\overline{\theta_l'^2 w'}$, $\overline{\theta_l' w'^2}$, $\overline{q_t'^2 w'}$, $\overline{q_t' w'^2}$, $\overline{w' q_t' \theta_l'}$, $\overline{\theta_l'^3}$, $\overline{q_t'^3}$, and $\overline{w'^4}$, are closed [*Larson and Golaz*, 2005]. In addition, buoyancy terms and cloud macrophysics quantities including cloud fraction and cloud liquid water mixing ratio are also computed from the assumed triple-joint PDF.

When CLUBB is configured in CAM5 (or SCAM5), it replaces the default planetary boundary layer (PBL), shallow cumulus and stratiform cloud macrophysics [*Park and Bretherton*, 2009; *Bretherton and Park*, 2009] as described in *Bogenschutz et al.* [2012]. SCAM5-CLUBB uses a two-moment cloud microphysics that predicts number and mass mixing ratios of cloud droplets and ice crystals and diagnoses number and mass mixing ratios of rain and snow as described by *Morrison and Gettelman* [2008~~, MG hereafter~~] and *Gettelman et al.* [2008, 2010]. The influence of aerosol on cloud microphysics is based on *Abdul-Razzak and Ghan* [2000] for the droplet activation and on *Liu et al.* [2007] for ice nucleation.

### 2.2. Single-Column Experiments

Three boundary layer cloud cases are analyzed to quantify the sensitivities of SCAM simulations to CLUBB parameter values (see section 2.3.1). The first two are shallow cumulus cases: the Barbados Oceanographic and Meteorological Experiment [BOMEX; *Siebesma et al.*, 2003], a trade wind cumulus regime, and the Rain in Cumulus Over Ocean [RICO, *Rauber et al.*, 2003], a precipitating shallow cumulus. The third case is the first aircraft research flight (RF01) of the Second Dynamics and Chemistry of Marine Stratocumulus Experiment (DYCOMS-II), a nonprecipitating marine stratocumulus case, hereafter referred to as DYCOMS-II RF01 [*Stevens et al.*, 2005]. AQ3

Because the vertical grid spacing is important to address sensitivities in CLUBB, SCAM5 with CLUBB has been configured at two different vertical resolutions (30 and 240 layers) for all three cases. The default configuration of CAM5 is 30 vertical levels; we also choose 240 vertical levels in order to investigate the sensitivity of CLUBB to the best-case vertical resolution. According to the quasi-Monte Carlo sampling approach (see section 2.3.2), each case with each resolution consists of an ensemble of multiple members.

Author Proof

### 2.3. SA Framework

#### 2.3.1. Tunable CLUBB Parameters

CLUBB is a complex and high-order system, which has 13 predictive equations (Appendix A) and about 50 contributing parameters. Most of its parameters are not peculiar to CLUBB. For example, parameters related to pressure terms of predictive equations, which were introduced by *André et al.* [1978] and *Bougeault* [1981], also appear in other high-order closure parameterizations that are based on *André et al.* [1978], including *Lappen and Randall* [2001], eddy kinetic energy model [*Gaspar et al.*, 1990], and *Cheng et al.* [2005]. Such a commonality in parameters allows this study to be a reference for other high-order closure schemes as well (see further discussions on this in section 4).

Sampling all parameters of CLUBB is computationally expensive if we extend SA study to global model in the future. Moreover, it does not benefit us to investigate which parameters and processes are the most influential ones when the number of parameters is large. It is therefore important to determine an appropriate number of parameters for the SA study.

The eddy diffusion terms have a unified form of $\frac{\partial\left[(K_w+\nu_X)\frac{\partial X}{\partial z}\right]}{\partial z}$, where X represents the prognostic field in each predictive equation (Appendix A), $\nu_X$ indicates background eddy diffusion coefficients associated with X; $K_w=c_{kX}\times c_k\times\ Lscale\times\ \sqrt{\bar{e}}$, where $\bar{e}$ is turbulence kinetic energy, *Lscale* is the eddy mixing length, $c_{kX}$ and $c_k$ are eddy diffusion coefficients. Based on the magnitude analysis, the eddy diffusion terms are found to be less important when compared with the pressure terms (including the Newtonian damping term and the buoyancy-damping term). Thus, we set the eddy diffusion coefficients ($\nu_X$, $c_k$, $c_{kX}$) to the same value in all predictive equations, and sample them uniformly. Thirty-five tunable parameters are then left as the full

 © 2014. The Authors. 

AGU Journal of Advances in Modeling Earth Systems 10.1002/2014MS000315

**Table 1.** CLUBB Parameters in the 16-Parameter Experiments[a] (See Table A1 for Parameters Used in the 35-Parameter Experiments)

| Tuning Parameter | Description | Default Value | Investigated Range |
|---|---|---|---|
| C1 | Low Skewness in C1 Skewness Function | 2.5 | 1.25–5 |
| C2rt | Constant associated with $\overline{r'_t{}^2}$ dissipation term | 1.0 | 0.5–2 |
| C2rtthl | constant associated with $\overline{r'_t\theta'_l}$ dissipation term | 1.0 | 0.5–2 |
| C6rt | Low Skewness in C6rt Skewness Function | 4.0 | 2.0–8.0 |
| C6rtb | High Skewness in C6thl Skewness Function | 6.0 | 2.0–8.0 |
| C7 | Low Skewness in C7 Skewness Function | 0.5 | 0.0–1.0 |
| C7b | High Skewness in C7 Skewness Function | 0.8 | 0.0–1.0 |
| C8 | Coefficient in C8 Skewness Equation | 3.0 | 1.5–6.0 |
| C11 | Low Skewness in C11 Skewness Function | 0.8 | 0.0–1.0 |
| C11b | High Skewness in C11 Skewness Function | 0.65 | 0.0–1.0 |
| C6_Lscale0 | Used to damp C6rt as a function of Lscale | 14.0 | 7.0–28.0 |
| C7_Lscale0 | Used to damp C7 as a function of Lscale | 0.85 | 0.425–1.7 |
| $\nu$ (nu) | Background Coefficient of Eddy Diffusion | 20.0 | 10.0–40.0 |
| $\beta$ (beta) | Constant related to "plume" variance of $\overline{\theta'_l{}^2}$ and $\overline{r'_t{}^2}$ | 1.75 | 0.0–3.0 |
| $\gamma$ (gamma_conf) | Low Skewness in $\gamma$ coefficient Skewness Function | 0.32 | 0.0–0.83 |
| $\mu$ (mu) | Parcel Entrainment Rate (Lscale) [1/m] | $1 \times 10^{-3}$ | $0.5–2.0 \times 10^{-3}$ |

[a]Texts in brackets are the names in source code of CLUBB.

set of parameters for the primary sensitive study. Their physical meanings are listed in Appendix A and Table A1. T3

However, 35 tunable parameters still require a considerable number of samples to produce reliable SA that would be computationally prohibitive when the study is extended to global simulation in the future. Therefore, we further reduce the number of parameters to 16 (listed in Table 1) by choosing those most influential parameters based on the relative contribution of each parameter in the 35-parameter simulations (see Appendix ~~B~~ A for more details). In addition, the 16-parameter experiment reduces the interferences of those parameters that are less important and leads to a better understanding of the influential ones. Actually, such a reduction on the number of the tunable parameters does not change our conclusions (see the discussion in section 4.1) and 16-parameter SA is therefore presented in section 3. T1 AQ4

Many of tunable parameters have clear and theoretical ranges. For example, $\gamma$ (gamma_coef, a dimensionless constant controls the widths of each individual Gaussian) spans from 0 to 1, while $\beta$ (beta, a dimensionless constant which controls the PDF parameters of total water and liquid water potential temperature) spans from 0 to 3 [*Larson and Golaz*, 2005]. Since the buoyancy-damping term should be less than the buoyancy term, coefficients associated with the buoyancy-damping term, including *C5*, *C7*, *C7b*, *C11*, and *C11b*, range from 0 to 1. The other parameters range from half to double their default values (listed in Table 1 and Table A1) for making a large parametric perturbation. Another factor in choosing the range of tunable parameters is numerical instability. As our tests show that a $\gamma$ larger than 0.83 can often cause numerical instability and lead to model crash, $\gamma$ is perturbed from 0 to 0.83 in this study.

### 2.3.2. Quasi-Monte Carlo Sampling

In this study, the probability distribution of each CLUBB parameter is assumed to be uniform within its uncertainty range (Table 1). Due to the high dimensionality of the parameter space, efficient and reliable SAs are necessary for the exploration of the parameter space and reduction of the dimensionality of model parameters. The choice of sampling technique is important as the success of a numerical approach hinges upon evaluating all possibilities defined by the model space. The quasi-Monte Carlo (QMC) sampling approach [*Caflisch*, 1998] is selected in our study. QMC guarantees a uniform distribution of sample points. When compared with the traditional Monte Carlo method, QMC improves sampling by filling gaps and avoiding clumps [*Hou et al.*, 2012].

### 2.3.3. Generalized Linear Model

A generalized linear model (GLM) is adopted to analyze the responses of cloud properties (including cloud fraction and liquid water mixing ratio) to the aforementioned CLUBB parameters, including their linear and nonlinear interaction effects. GLM assumes that the response of cloud properties is a function of these CLUBB parameters:

 © 2014. The Authors. 

AGU Journal of Advances in Modeling Earth Systems 10.1002/2014MS000315

$$Y=\beta_0+\sum_{j=1}^{n}\beta_j*p_j+\sum_{j=1}^{n}\sum_{j=1}^{n}\beta_{j,k}*p_j*p_k+\varepsilon,\quad \varepsilon\sim N(0,\sigma^2) \tag{1}$$

where $Y$ represents the response variable (e.g., cloud fraction); $p_j$ represents the $j$th parameter; $\beta_j$ and $\beta_{j,k}$ represent the coefficients of linear and two-way interaction terms; and $\varepsilon$ denotes the residual and follows independent normal distributions with zero mean and unit variance.

The SA quantifies the simulated variations of cloud properties that results from perturbations of CLUBB parameters and identifies the significant parameters that contribute to these variations. GLM builds fitting equations, through maximum likelihood estimation between parameters ($p$) and simulations ($Y$). The GLM computes coefficient of determination ($R^2$) of model fitness, interpreted variance and the P-value of each parameter. The reduction in the residual sum square caused by each parameter is used to calculate its relative contributions [*McCullagh and Nelder*, 1989]. The P-value is the probability of obtaining a test statistic AQ5 result at least as extreme as the one that was actually observed, assuming that the null hypothesis $H$ is true (here the null hypothesis is that the contribution of a parameter to the total variation in cloud properties is insignificant). The P-value is calculated as the conditional probability $\Pr(|T|\geq t|H)$, where T is t-statistic and t is an instant. When the P-value of a parameter is smaller than $1-\alpha$, where $\alpha$ is a chosen significance level (95% is chosen for this study), the null hypothesis is rejected and the parameter is regarded as a significant contributor. More details of GLM have been described in *McCullagh and Nelder* [1989].

#### 2.3.4. Evaluation Metric

Following *Taylor* [2001] and *Yang et al.* [2013], a cost function based on the spatial standard deviations and spatial correlations is used as a metric to evaluate SCAM5 results against the large-eddy simulations (LES) [*Golaz et al.*, 2005]. LES are used as a benchmark for comparisons with the SCAM. The same LES results have also been used in *Bogenschutz et al.* [2012].

$\sigma_x$ is the standard deviation of simulated variable (x) and is calculated as follows:

$$\sigma_x=\sqrt{\frac{1}{N}\sum_{i=1}^{N}(x_i-\bar{x})^2} \tag{2}$$

where $i$ is the index for vertical layer, $N$ is the number of vertical grid point, and the $\bar{x}$ is the vertical mean of variable $x$. The correlation coefficient $R$ between $x$ and LES variable ($y$) is defined as

$$R=\frac{\frac{1}{N}\sum_{i=1}^{N}(x_i-\bar{x})(y_i-\bar{y})}{\sigma_x\sigma_y} \tag{3}$$

where $\bar{y}$ is the vertical mean of variable $y$.

The performance score ($scr$) is then defined as

$$scr=\log\left[\frac{\left(\frac{\sigma_y}{\sigma_x}+\frac{\sigma_x}{\sigma_y}\right)^2(1+R_0)^k}{4(1+R)^k}\right] \tag{4}$$

where $R_0$ and $k$ are maximum possible spatial correlation coefficient and specified values used to control the relative weight of spatial correlation. Following *Yang et al.* [2013], we set $R_0=1$ and $k=4$. Smaller $scr$ means the simulation matches LES better in terms of vertical cloud profiles. Note that LES outputs are interpolated onto the same vertical resolution with simulations. Here the vertical profile of cloud fraction is chosen for evaluating SCAM5 simulations, because the vertical profile of cloud fraction in shallow cumulus is more challenging to capture than the vertical profile of cloud water (not shown).

## 3. Results

### 3.1. Stratocumulus

#### 3.1.1. Results of Generalized Linear Model

Figure 1 shows the anomalies of total cloud fraction (derived by maximum-random overlap assumption) F1 averaged over hours 3–4 in response to the perturbations of 16 parameters from the 256 low-resolution (30


© 2014. The Authors.


ID: kandasamy.d Time: 18:43 I Path: N:/3b2/JAME/Vol00000/140037/APPFile/JW-JAME140037

AGU Journal of Advances in Modeling Earth Systems 10.1002/2014MS000315

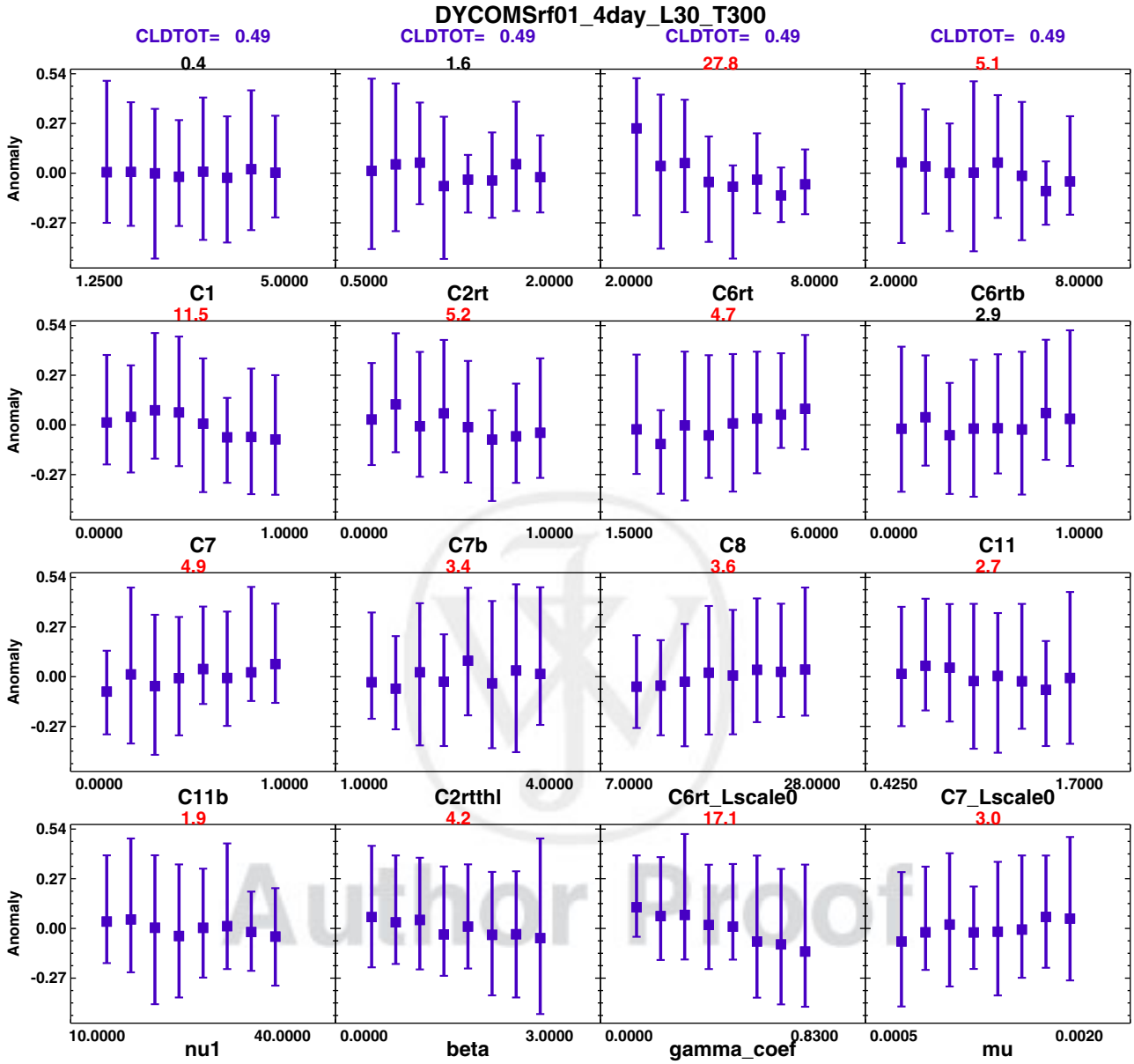


**Figure 1.** Anomalies of variation of total cloud fraction averaged over hours 3 and 4 in response to the perturbations of 16 parameters from the 256 SCAM5-CLUBB DYCOMSII RF01 simulations. The vertical resolution of SCAM5-CLUBB is 30 layers (L30). The mean total cloud fraction of 256 simulations is shown as CLDTOT. The numbers above each plot box represent the relative contribution (percentage) of each input parameter perturbation to the overall cloud fraction variations. Red means the contribution with 95% statistic significance. The mean is denoted as boxes, while the vertical bars show the range of cloud fraction anomaly from tenth percentile (lower) to ninetieth percentile (upper).

vertical layers) DYCOMS-II RF01 simulations. These 256 simulations are equally grouped into 8 bins for each input parameter. The anomalies are calculated by subtracting the mean of 256 simulations (49% for low-resolution DYCOMS-II) from each individual simulation. The range of cloud fraction in each bin of an individual input parameter results from perturbations of other parameters because the parameters are perturbed simultaneously during the sampling.

Figure 1 shows how cloud properties respond to those perturbations of CLUBB parameters. A large spread of cloud fraction anomalies from −48% to +51%, corresponding to cloud fractions from 0.01 to 1, is seen in Figure 1 in response to the perturbations of the 16 CLUBB parameters. In addition, the numbers above each plot represent the relative contribution of each parameter perturbation to the overall variations of cloud properties. Numbers highlighted in red indicate that the contributions of the corresponding parameters to the total variance are statistically significant with 95% confidence level. The perturbation in *C6rt* contributes


© 2014. The Authors.

AGU Journal of Advances in Modeling Earth Systems 10.1002/2014MS000315

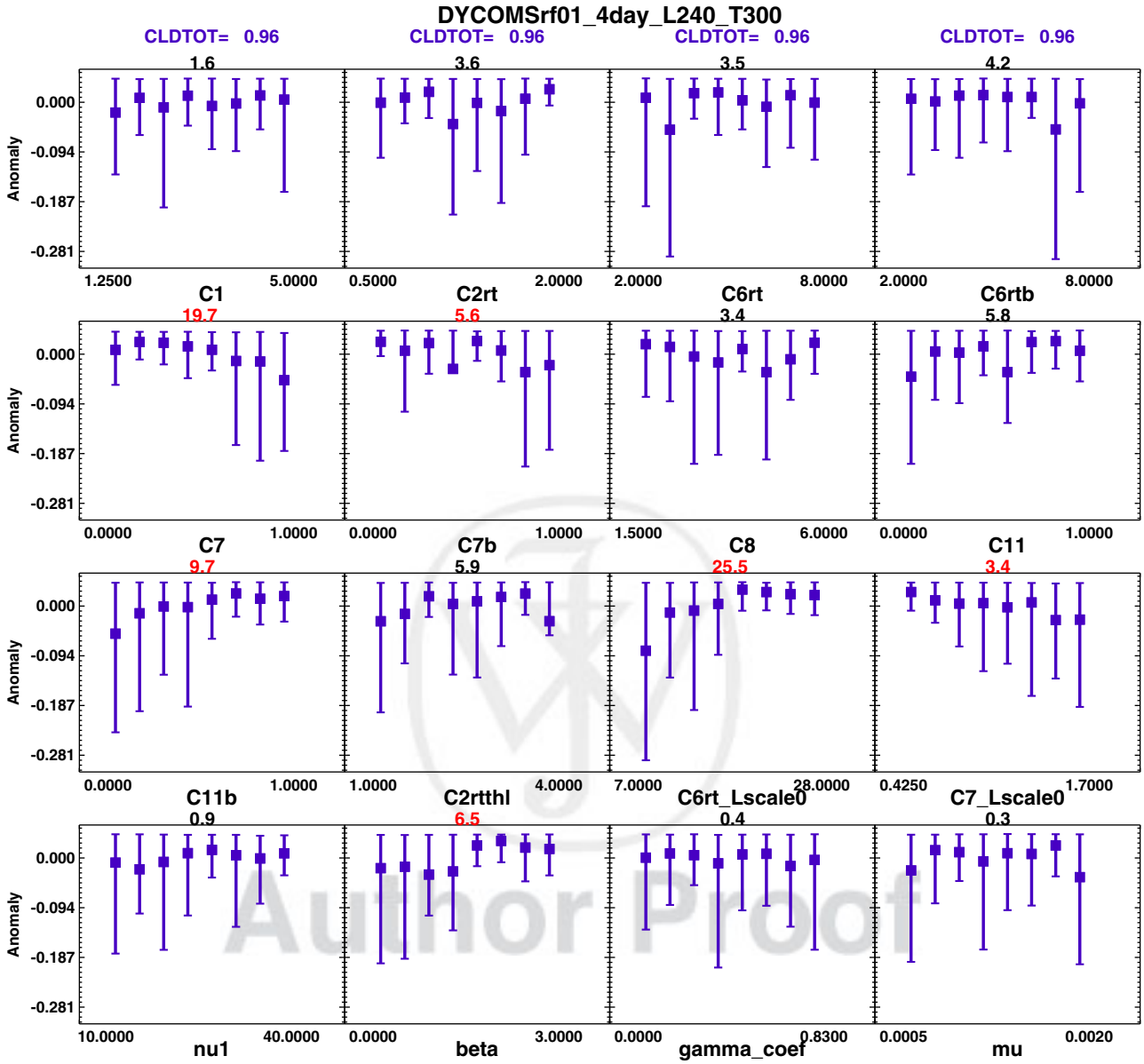


**Figure 2.** Same as Figure 1, but at high vertical resolution (240 layers, L240).

the most (27.8%) to the total variance of cloud fraction, followed by that of *C7* (11.5%), *C7b* (5.2%), *C6b* (5.2%), and $\gamma$ (17.1%). Contributions from the perturbations in another 10 CLUBB parameters are also statistically significant (with 95% confidence level), although their contributions are small (less than 5%). In the low vertical resolution simulation of DYCOMS-II RF01, cloud fraction generally decreases with increasing *C7*, *C6rt*, and $\gamma$.

Results from the high vertical resolution (240 vertical layers) simulations are shown in Figure 2 and are different from the results from the low resolutions. The ensemble mean cloud fraction is 96%, much higher than that at low vertical resolution (49%) and closer to the reference LES simulation (91%). *C6rt*, which contributes the most to the cloud fraction variation at low resolution, becomes much less important with its contribution of 3.5%. Its dominance is replaced by *C6rt_Lscale0* (contribution of 25.5%), as shown in Figure 2. Compared with low resolution, C7 is still one of the largest contributors (19.7%). As in low-resolution simulations, cloud fraction somewhat decreases with *C7*. However, cloud fraction increases with *C6rt_Lscale0*, in contrast to the low-resolution results.


© 2014. The Authors.

AGU Journal of Advances in Modeling Earth Systems 10.1002/2014MS000315

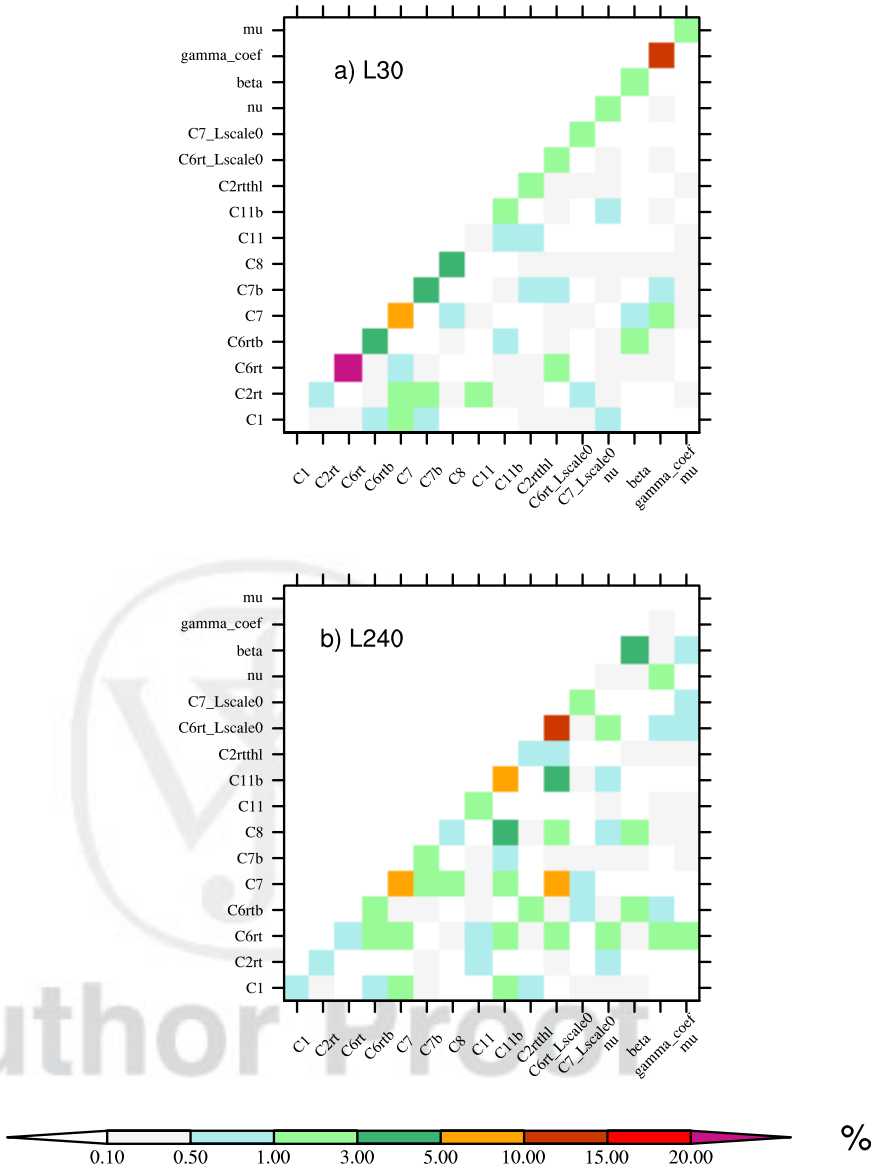


**Figure 3.** Relative contributions (percentage, shading) of interactions of tunable parameters to the variations of total cloud fraction estimated by the Generalized Linear Model in DYCOMSII RF01: (a) at low vertical resolution simulation (30 layers), with $R^2$ of 0.95 (0.72 from individual terms); (b) at high vertical resolution (240 layers), with $R^2$ of 0.94 (0.55 from individual terms).

As shown in Figure 3, the interactions among the 16 tunable parameters can also be quantified, which indicate the effects of nonlinear coupling of different parameters. The interactions mean the effects caused by the initial perturbation of one parameter will be amplified or suppressed by the other parameters compared to its one-at-a-time sensitivity [*Zhao et al.*, 2013]. Most of the interaction effects among the selected 16 input parameters are inconsequential with magnitude less than 3%, compared with the effects of individual parameters, except for *C7* to *C6rt_Lscale0* at high resolution.

The GLM fits the simulated cloud fraction well with the coefficients of determination ($R^2$) of 0.95 at low resolution and 0.94 at high resolution, which indicate 95% and 94% of variance of SCAM5-CLUBB simulated cloud fraction can be explained by the GLM. The individual parameters contribute a $R^2$ of 0.72 to the total $R^2$ of 0.95 at low resolution and 0.55 to the total $R^2$ of 0.94 at high resolution. Although the contributions of most interactions are small in magnitude compared to the contributions from individual parameters, the large amounts of interaction terms ($120 = 16 \times 15/2$) make their total contribution notable.


© 2014. The Authors.

AGU Journal of Advances in Modeling Earth Systems 10.1002/2014MS000315

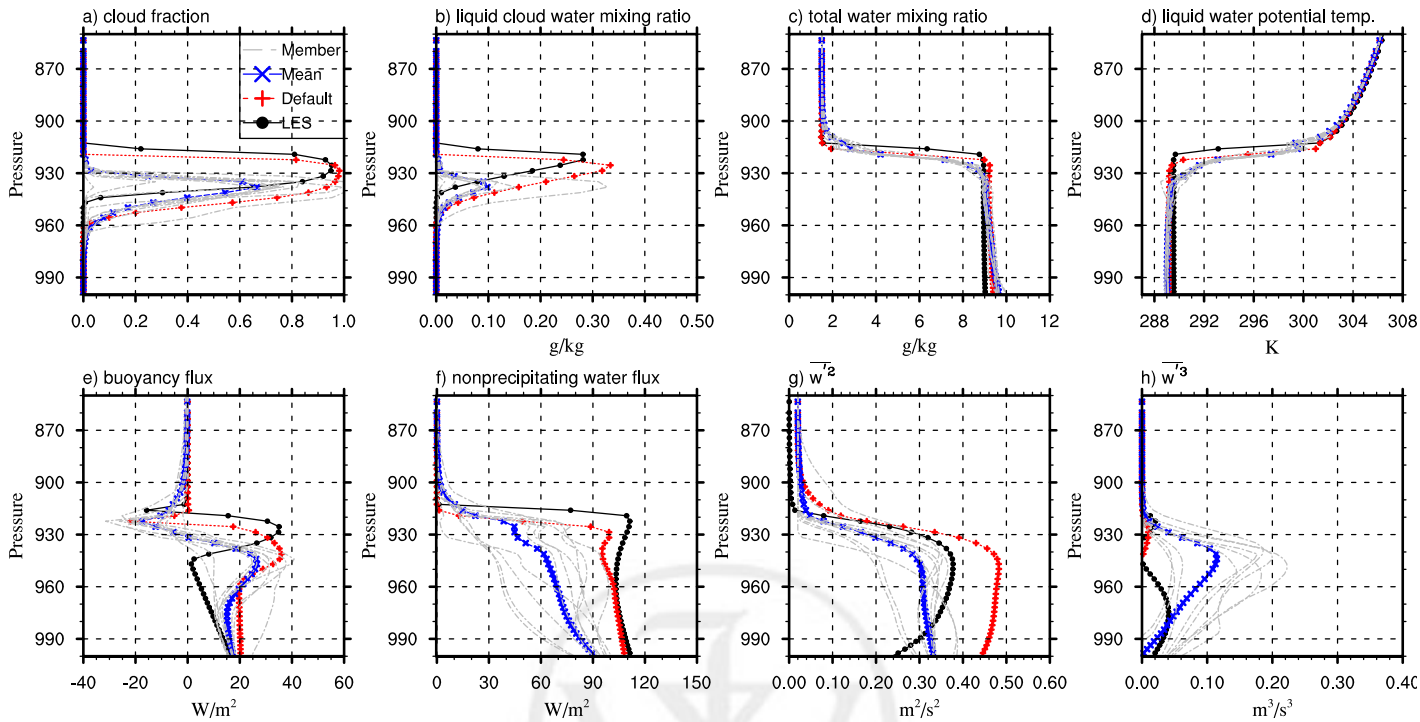


**Figure 4.** Mean vertical profiles of top 10 poor performance samples for the DYCOMSII RF01 case at high vertical resolution (240 layers), averaged over hours 3–4: (a) cloud fraction, (b) liquid cloud water mixing ratio (g/kg), (c) total water mixing ratio (g/kg), (d) liquid water potential temperature (K), (e) buoyancy flux (W/m$^2$), (f) nonprecipitating water flux (W/m$^2$), (g) variance of vertical velocity ($\overline{w'^2}$, m$^2$/s$^2$), and (h) third-order moment of vertical velocity ($\overline{w'^3}$, m$^3$/s$^3$). The gray lines represent the individual samples (10), and the blue lines show average of those samples. The red lines indicate the LES results. The black lines indicate the profiles with the default parameter values.

### 3.1.2. Discussion of Sensitive Parameters and Their Physical Meaning

To better understand which processes contribute most to cloud fraction variations and why those aforementioned parameters are influential, vertical profiles of model fields from 10 SCAM5-CLUBB simulations at high resolution with lowest and highest performance scores (scr) (see the definition in section 2.3.3) based on the vertical profile of cloud fraction are analyzed and compared against the reference LES (Figures 4 and 5).

LES predicts an inversion-capped mixed-layer structure with a nearly overcast cloud located between 915 hPa and 940 hPa (Figure 4, black). The buoyancy flux decreases linearly in the subcloud layer up to the cloud base with relatively small buoyancy fluxes located at the cloud base. In addition, a single well-defined peak of $\overline{w'^2}$ is also seen near the cloud base, and the third moment of vertical velocity $\overline{w'^3}$ is small due to the near symmetry between updraft and downdraft in stratocumulus.

The simulated inversion and boundary structure depends on details of the turbulent mixing. Compared to the LES, the "poor performance" SCAM-CLUBB runs are unable to reproduce the LES profiles in DYCOMS-II RF01 (Figure 4, blue and gray). All poor performance simulations have relatively large gradients in $\bar{\theta}_l$ and $\bar{q}_t$ in the mixed layer. Liquid cloud water mixing ratio ($\bar{q}_c$) and cloud fraction are largely underestimated in these samples. These biases are related to the relatively unrealistic simulation of boundary layer conditions. First, these samples are unable to produce a well-mixed $\bar{\theta}_l$ and $\bar{q}_t$, which indicates poor and weak boundary layer mixing processes (see the total water flux in Figure 4f). Second, the negative buoyancy at cloud top and positive buoyancy near the cloud base are too weak, even negative in some samples and the ensemble mean (Figure 4e, gray and blue). Such structures of buoyancy allow the occurrence of strong entrainment in cloud top and decoupling near cloud base, which leads to low stratocumulus cloud fraction.

For the "good performance" SCAM_CLUBB simulations (Figure 5), the cloud properties of SCAM-CLUBB and LES appear comparable. Although some significant overestimations are present in even "good performance" runs, they compare well with LES. The well-mixed profile of liquid water potential temperature is reproduced, although the well-mixed profile of total water is less accurately reproduced. In a buoyantly


© 2014. The Authors.

AGU Journal of Advances in Modeling Earth Systems 10.1002/2014MS000315

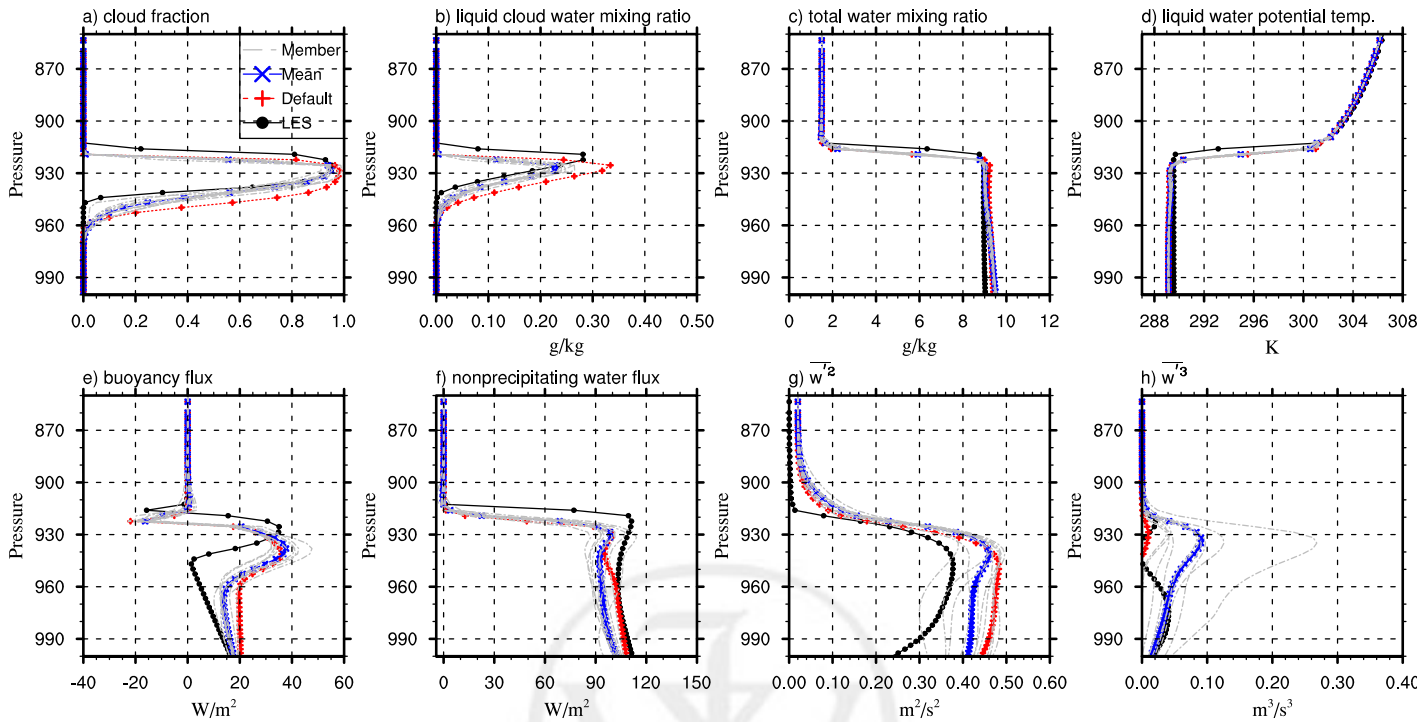


**Figure 5.** Same as Figure 4, but for top 10 good performance samples.

driven turbulent layer, liquid water potential temperature is more constrained by buoyancy to be well mixed, whereas total water is less constrained.

For simulated stratocumulus, the cloud fraction is most sensitive to *C7* and *C6rt* parameters. Both of them influence the turbulence fluxes of liquid water potential temperature ($\overline{w'\theta'_l}$) and total water mixing ratios ($\overline{w'q'_t}$) through the skewness function ($C_{6sk}$, $C_{7sk}$). $C_{6sk}$ is defined as

$$C_{6sk}=\begin{cases} C6rt_Lscale+\dfrac{C_{6rtb}+(C_{6rt}-C_{6rtb})e^{-0.5\times\left(\frac{Skw}{C_{6rtc}}\right)^2}-C6rt_Lscale}{wpxp_L_thresh}\times Lscale; & (Lscale<wpxp_L_thresh) \\ C_{6rtb}+(C_{6rt}-C_{6rtb})e^{-0.5\times\left(\frac{Skw}{C_{6rtc}}\right)^2} & (Lscale>wpxp_L_thresh) \end{cases} \tag{5}$$

where *Lscale* is the eddy mixing length (discussed later) and *Skw* represents skewness of the vertical velocity. $C_{7sk}$ is defined in a similar way. *Skw* is defined as

$$Skw=\frac{\overline{w'^3}}{(\overline{w'^2}+Skw_demon_coef\times\overline{w'^2}|_{tol})^{1.5}} \tag{6}$$

in which $\overline{w'^2}|_{tol}$ (a constant of 0.0004 m$^2$/s$^2$) is the threshold for vertical velocity variance $\overline{w'^2}$. Here *C6rt* and *C6rtb* are included in the 16-parameter experiments (Table 1), while *Skw_demon_coef* and *C6rtc* are included in the 35-parameter experiments (Appendix B and Table A1).

The turbulence fluxes of liquid water potential temperature ($\overline{w'\theta'_l}$) and total water mixing ratios ($\overline{w'q'_t}$) [*Golaz* ~~*and Larson, 2001*~~; *Larson and Golaz*, 2005; *Golaz et al.*, 2007] are predicted as


© 2014. The Authors.


ID: kandasamy.d Time: 18:43 I Path: N:/3b2/JAME/Vol00000/140037/APPFile/JW-JAME140037

AGU Journal of Advances in Modeling Earth Systems 10.1002/2014MS000315

$$\frac{\partial \overline{w'q'_t}}{\partial t} = -\bar{w}\frac{\partial \overline{w'q'_t}}{\partial z} - \frac{1}{\rho_s}\frac{\partial \rho_s \overline{w'^2 q'_t}}{\partial z} - \overline{w'^2}\frac{\partial \bar{q}_t}{\partial z} - \overline{w'q'_t}\frac{\partial \bar{w}}{\partial z} + \frac{g}{\theta_{vs}}\overline{q'_t\theta'_v} - \frac{C_{6sk}}{\tau}\overline{w'q'_t}$$
$$+ C_{7sk}\overline{w'q'_t}\frac{\partial \bar{w}}{\partial z} - C_{7sk}\frac{g}{\theta_{vs}}\overline{q'_t\theta'_v} + \frac{\partial\left[(K_w+\nu)\frac{\partial \overline{w'q'_t}}{\partial z}\right]}{\partial z} + \left.\frac{\partial \overline{w'q'_t}}{\partial t}\right|_{sicl} \tag{7}$$
$$+ \left.\frac{\partial \overline{w'q'}}{\partial t}\right|_{cl} + \left.\frac{\partial \overline{w'q'}}{\partial t}\right|_{mfl}$$

$$\frac{\partial \overline{w'\theta'_l}}{\partial t} = -\bar{w}\frac{\partial \overline{w'\theta'_l}}{\partial z} - \frac{1}{\rho_s}\frac{\partial \rho_s \overline{w'^2\theta'_l}}{\partial z} - \overline{w'^2}\frac{\partial \bar{\theta}_l}{\partial z} - \overline{w'\theta'_l}\frac{\partial \bar{w}}{\partial z} + \frac{g}{\theta_{vs}}\overline{\theta'_l\theta'_v} - \frac{C_{6sk}}{\tau}\overline{w'\theta'_l}$$
$$+ C_{7sk}\overline{w'\theta'_l}\frac{\partial \bar{w}}{\partial z} - C_{7sk}\frac{g}{\theta_{vs}}\overline{\theta'_l\theta'_v} + \frac{\partial\left[(K_w+\nu)\frac{\partial \overline{w'\theta'_l}}{\partial z}\right]}{\partial z} \tag{8}$$
$$+ \left.\frac{\partial \overline{w'\theta'_l}}{\partial t}\right|_{sicl} + \left.\frac{\partial \overline{w'\theta'_l}}{\partial t}\right|_{cl} + \left.\frac{\partial \overline{w'\theta'_l}}{\partial t}\right|_{mfl}$$

where the subscript *sk* indicates coefficients that are not constant but parameterized as functions of skewness of the vertical velocity distribution to better differentiate stratocumulus from shallow cumulus [*Golaz et al.*, 2007], as shown in equation (5).

The C7 skewness function ($C_{7sk}$) works in terms that are proportional to $\frac{\partial \bar{w}}{\partial z}$ and the damping terms of buoyancy moment ($\overline{\theta'_l\theta'_v}$ and $\overline{q'_t\theta'_v}$). As the former is negligible in magnitude, terms related to the C7 skewness function mainly act as a sink of scalar fluxes related to buoyancy. In the stratocumulus case, the boundary layer is capped by a sharp and strong inversion. This inversion blocks the rising eddies and spreads their kinetic energy horizontally. Strong buoyancy usually occurs at the upper portion of the cloud layer (near the inversion) and weakens the entrainment and mixing at cloud top. From equations (7) and (8), decreasing C7 increases the buoyancy moment at the cloud top and cloud base and then enhances the turbulence fluxes. Those are favorable for increasing cloud fraction and cloud water mixing ratio. It is consistent with SA that the tight coupling between cloud-layer mixing and C7 skewness function is the likely cause of stratocumulus preference for lower values of C7 skewness function and C7.

The effect of *C6rt*, the largest contributor to the variance of cloud fraction at low resolution, is different from that of *C7*. It controls the Newtonian damping term ($-\frac{C_{6sk}}{\tau}\overline{w'q'_t}$ and $-\frac{C_{6sk}}{\tau}\overline{w'\theta'_l}$) in the turbulence flux equations (equations (7) and (8)). The Newtonian damping term always acts as a sink of prognostic turbulence fluxes. Its magnitude is determined by both the C6 skewness function and the dissipation time scale $\tau$, which are largely determined by the vertical structure of the boundary layer. It makes the effects of the Newtonian damping term more complex to understand than the buoyancy-damping term.

The definition of $\tau$ is [*Golaz et al.*, 2002a]

$$\tau = \frac{Lscale}{\sqrt{\bar{e}}} \tag{9}$$

where $\bar{e}$ is turbulence kinetic energy. Near the inversion, *Lscale* (Figure 6a) and consequently the dissipation time scale $\tau$ is small (Figure 6b), because of the capped inversion that determines the maximum size of eddy at a distance. Thus, the peak of the Newtonian damping term ($-\frac{C_{6sk}}{\tau}\overline{w'q'_t}$ and $-\frac{C_{6sk}}{\tau}\overline{w'\theta'_l}$) tends to locate near inversion layer (Figure 6d).

In a stably stratified layer (near the inversion, see Figure 6a), $C_{6sk}$ is further modified as a function of eddy mixing length *Lscale* in order to block gravity wave, as shown in equation (5). As the vertical structure of the inversion (or *Lscale*) strongly depends on vertical resolution (Figure 6a), the effect of the Newtonian damping term can be different at low and high resolutions. At coarse resolution (e.g., L30, L60), *Lscale* and dissipation times are underestimated at 925–950 hPa and are overestimated above 925 hPa (Figures 6a and 6b). The overestimation above 925 hPa produces a stronger dissipation of water flux in the mixing layer (Figure 6d), which leads to low cloud fraction. As the vertical resolution increase from 30 to 240 levels, the boundary layer structure is better simulated and cloud fraction increases.


© 2014. The Authors.

AGU Journal of Advances in Modeling Earth Systems 10.1002/2014MS000315

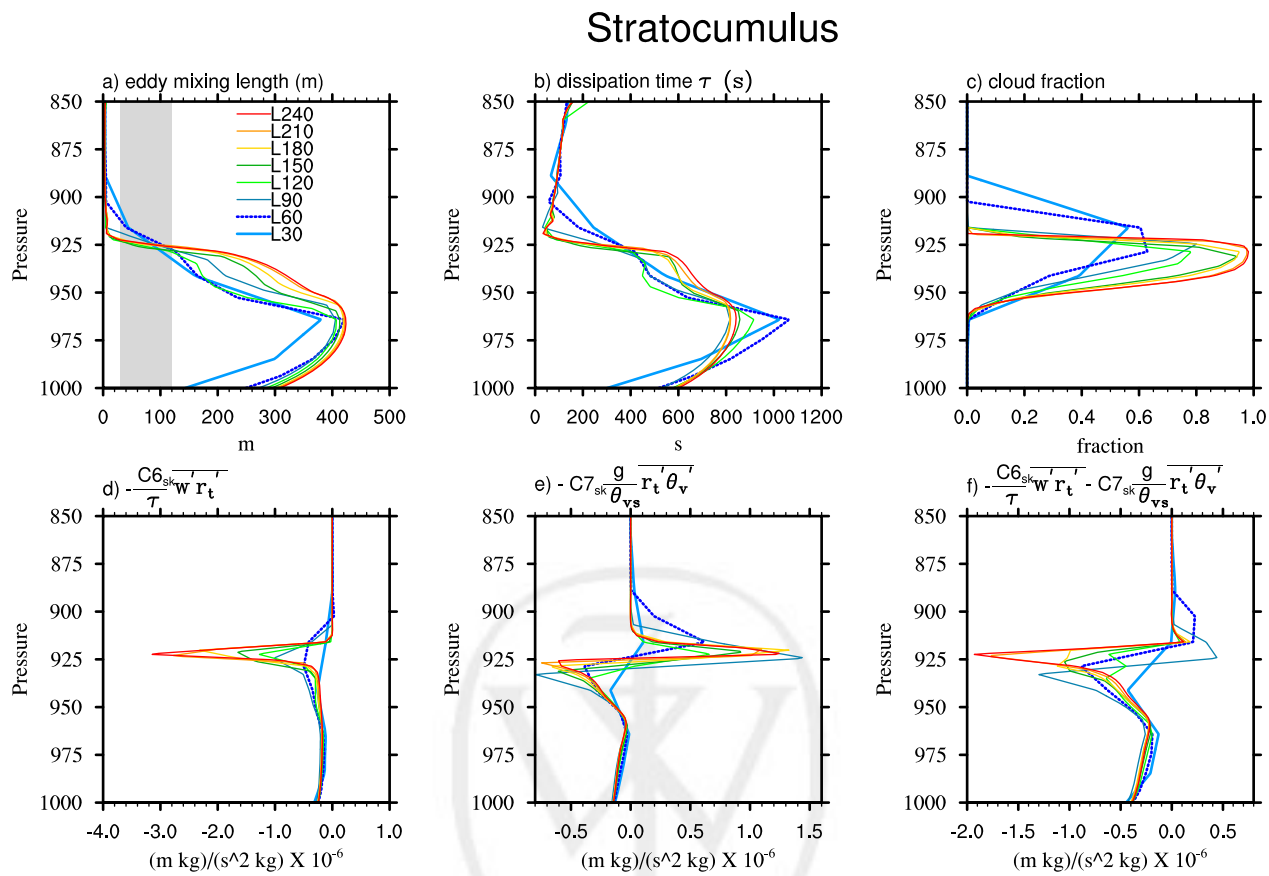


**Figure 6.** Mean vertical profiles (averaged over hours 3–4) for the DYCOMSII RF01 simulation with the default parameter values: (a) eddy mixing length *Lscale* (m), (b) dissipation time $\tau$ (s), (c) cloud fraction (%), (d) Newtonian term of total water flux (m kg/kg/s$^2$), (e) buoyancy-damping term of total water flux (m kg/kg/s$^2$), and (f) the sum of Newtonian term and buoyancy-damping term (m kg/kg/s$^2$). Different colors represent different resolutions (8 in total, from 30 vertical layers (L30) to 240 vertical layers (L240)) and the shading in (a) represents the tunable ranges of *wpxp_L_thresh* in the 35-parameter experiments.

Because the low vertical resolution SCAM5 simulations don't capture the large gradient of *Lscale* at the top of boundary layer well (Figure 6a), it is hard to get the criterion that *Lscale* is less than its threshold wpxp_L_thresh, which is fixed at 60 m here (wpxp_L_thresh is included as a tunable parameter in the 35-parameter experiments with a range of 30–120 m, see shading in Figure 6a and Table A1). Therefore, C6rt dominates the skewness function of C6 in the total water turbulence fluxes ($\overline{w'q'_t}$). At high resolution, however, the criterion is easier to meet and therefore C6rt_Lscale0 replaces C6rt as controller of the C6 skewness function at the top of boundary layer.

At low resolution, the peak of the Newtonian damping term locates in the cloud layer and at cloud base due to the crude boundary layer structure (Figures 6c and 6d). It mainly weakens the fluxes in the cloud layer, which causes a tight negative coupling between cloud-layer mixing and the C6 skewness function (*C6rt*). However, at high resolution, the Newtonian damping term with its peak located at the inversion layer blocks the fluxes at cloud top, reduces entrainment, and preserves the well-mixed boundary layer. Thus, stratocumulus clouds prefer larger values of *C6rt_Lscale0* and C6 skewness function at high resolution. Unlike the Newtonian damping term, the buoyancy-damping term has the same effect at low and high resolutions (Figure 6e). Thus, *C7_Lscale0* just replaces *C7* partly with increasing vertical resolution.

As shown in Figure 3b, the interaction of *C6rt_Lscale*0 and *C7* is notable at high resolution while negligible at low resolution. For high-resolution simulations, the buoyancy-damping term that controlled by *C7* compensates Newtonian damping term in cloud layer (Figures 6d–6f). Therefore, their interaction is notable at high resolution. The other change related to the changing of vertical resolution is the relative contribution of $\gamma$, which affects the cloud fraction more at low resolution (Figure 3). The possible reason is that $\gamma$ controls the weight of the two Gaussian distributions (see more details in the next section) that are quite different at low resolution while similar at high resolution (not shown).


© 2014. The Authors.

AGU Journal of Advances in Modeling Earth Systems 10.1002/2014MS000315

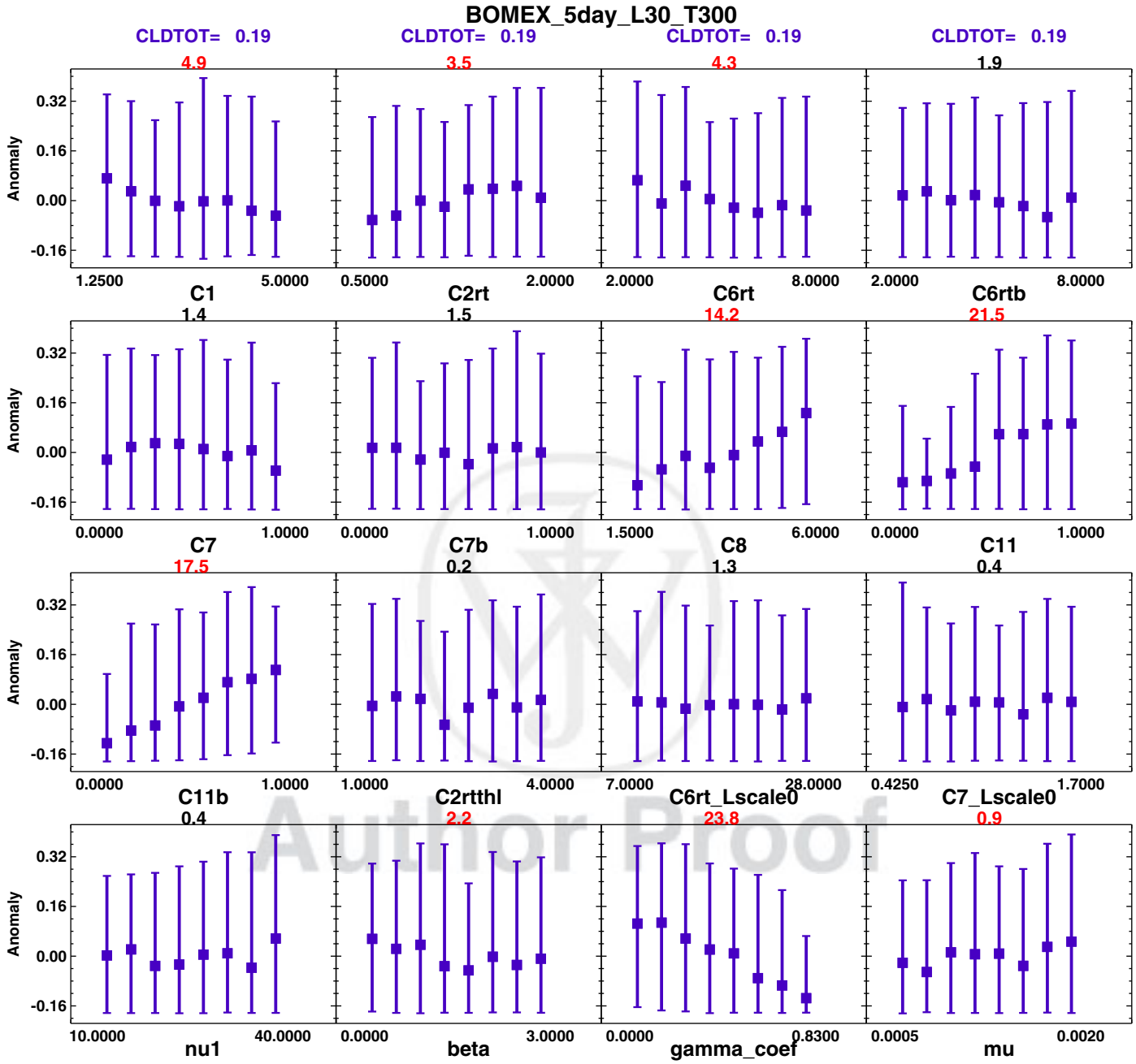


**Figure 7.** Anomalies of variation of total cloud fraction averaged over hours 5 and 6 in response to the perturbations of 16 parameters from the 256 SCAM5-CLUBB BOMEX simulations. The vertical resolution of SCAM5-CLUBB is 30 layers. The mean total cloud fraction of 256 simulations is shown as CLDTOT. The numbers above each plot box represent the relative contribution (percentage) of each input parameter perturbation to the overall cloud fraction variations. Red means the contribution with 95% statistic significance. The mean is denoted as boxes, while the vertical bars show the range of cloud fraction anomaly from tenth percentile (lower) to ninetieth percentile (upper).

### 3.2. Shallow Convection

#### 3.2.1. Results of Generalized Linear Model

Figure 7 shows the anomalies of total cloud fraction averaged over hours 5–6 in response to the perturbations of the 16 parameters from the low-resolution BOMEX simulations. The perturbation of $\gamma$ is the largest contributor (23.8%) to the total variance of cloud fraction, followed by that of *C11* (21.8%), *C11b* (17.5%), *C8* (14.2%), and other parameters with contributions less than 5%. The high resolution shares similar contributors with the low resolution, with somewhat different magnitudes (Figure 8). The perturbations of $\gamma$ (21.1%), *C11b* (22.3%), *C11* (14.1%), and *C8* (12%) are still the largest contributors.


© 2014. The Authors.

AGU Journal of Advances in Modeling Earth Systems 10.1002/2014MS000315

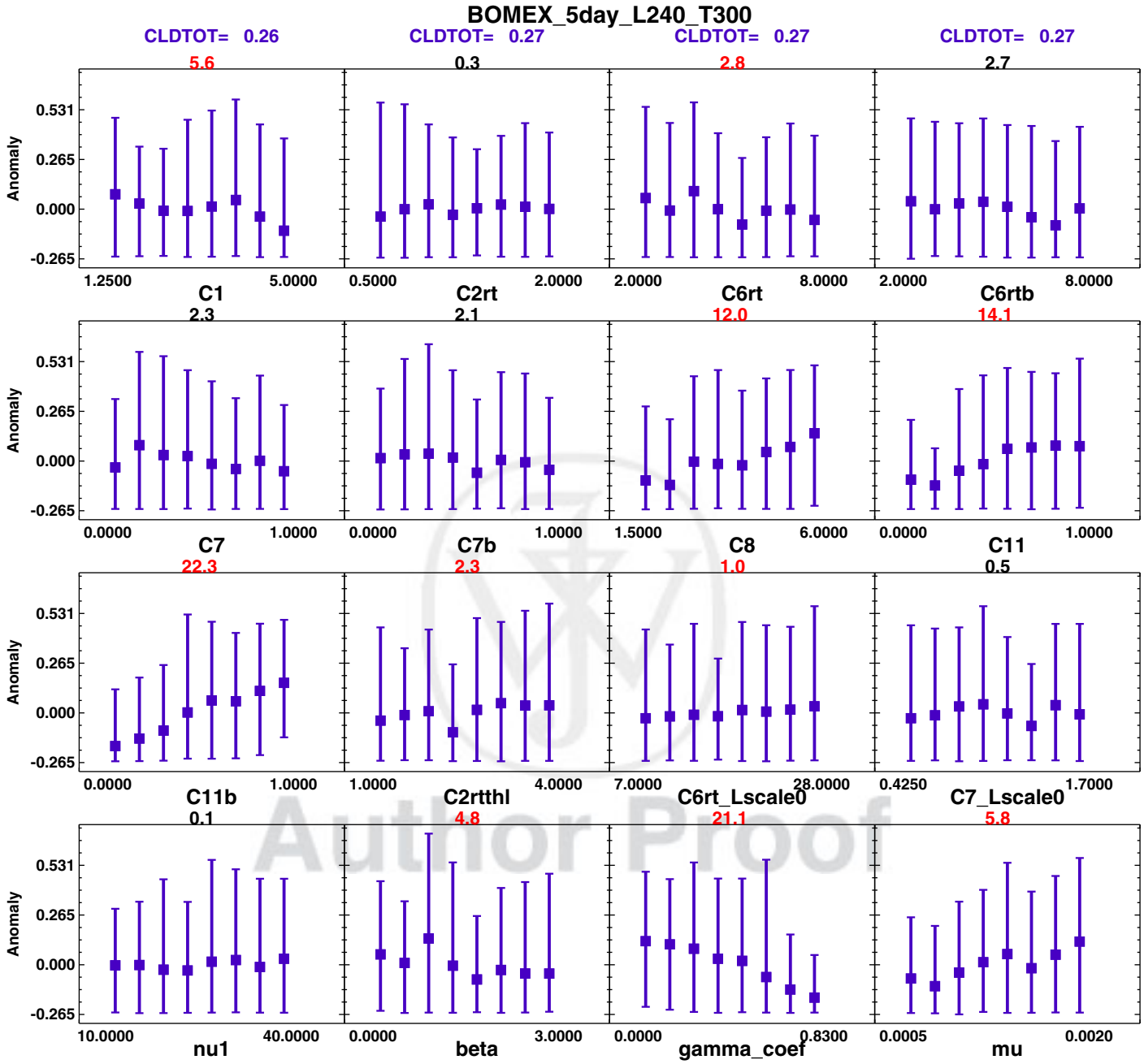


**Figure 8.** Same as Figure 7, but at high vertical resolution (240 layers).

In general, large spread of cloud fraction is seen in Figures 7 and 8, which ranges from 3% to 58% in response to the perturbations of the 16 CLUBB parameters. Cloud fraction increases with *C11b*, *C11*, and *C8*, but decreases with $\gamma$ and $\beta$. All these large contributors are related to the third moment of vertical velocity and PDF closure, which will be discussed later. In addition, the sensitive parameters for the precipitating marine shallow cumulus for the Rain in Cumulus Over Ocean (RICO) experiment are similar to those for BOMEX at both resolutions, except some small differences in their relative contributions, especially at high resolution (Figure 9).

Similar to the analysis of interaction effects for DYCOMS-II RF01 (Figure 3), the individual and interaction effects analyzed using the GLM are shown in Figure 10. In BOMEX, the individual effects dominate the total effect and the interaction effect is relatively small. Most of the interaction effects among the selected 16 input parameters are inconsequential with magnitude less than 1. The GLM fits the simulations in cloud


© 2014. The Authors.

AGU Journal of Advances in Modeling Earth Systems 10.1002/2014MS000315

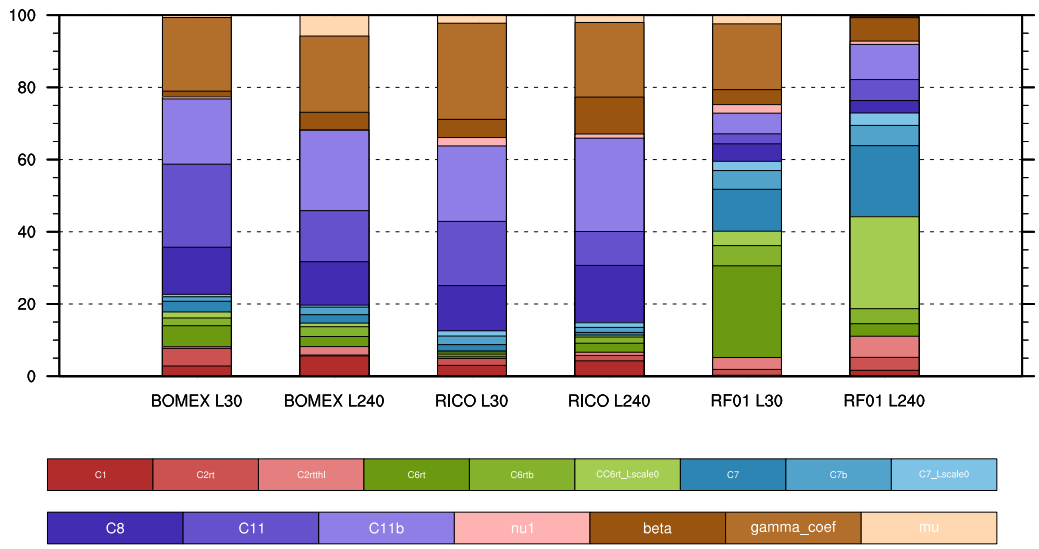


**Figure 9.** The relative contributions of individual parameters to the overall cloud fraction variations in the 16-parameter experiments from two shallow convection cases (BOMEX averaged over hours 5–6 and RICO averaged over hours 7–8) and one stratocumulus case (DYCOMS-II RF01 averaged over hours 3–4) at low (30 vertical layers, L30) and high (240 vertical layers, L240) resolutions.

fraction well with the coefficients of determination ($R^2$) of 0.97 at low resolution and 0.94 at high resolution. Among the total $R^2$, 0.77 is contributed by individual parameters at low resolution and 0.7 at high resolution.

### 3.2.2. Discussion of Sensitive Parameters and Their Physical Meaning

Similar to DYCOMS-II RF01, profiles from the 10 BOMEX simulations with the lowest and highest performance scores (based on the vertical profile of cloud fraction) are shown in Figures 11 and 12, respectively. In LES, cloud fraction is small with its peak located at cloud base (Figure 12a). The negative buoyancy fluxes near cloud base indicate an evident decoupling and the PBL remains poorly mixed with double well-defined peaks in $\overline{w'^2}$ near cloud base. The positive third-order moment of vertical velocity $\overline{w'^3}$ is characteristic of cumulus convection, which means narrow and strong updrafts that are compensated by broad and weak downdrafts. There is a strong correlation between variations in cloud properties, turbulence, $\overline{w'^3}$, and subcloud buoyancy fluxes. Simulations that produce unrealistic cloud fraction also tend to produce larger positive buoyancy fluxes near cloud base and smaller $\overline{w'^3}$ (and vertical velocity skewness) within the boundary layer (Figure 11), and vice versa. This indicates that the skewness of vertical velocity is the key to the simulation of shallow cumulus. This is consistent with the influential parameters identified using GLM that are related to the skewness of vertical velocity, such as *C11*, $\gamma$, *C11b*, and *C8*.

*C8*, *C11*, and *C11b* control the pressure correlation term of $\overline{w'^3}$:

$$\begin{aligned}\frac{\partial\overline{w'^3}}{\partial t} &= -\bar{w}\frac{\partial\overline{w'^3}}{\partial z} - \frac{1}{\rho_s}\frac{\partial\overline{w'^4}}{\partial z} + 3\frac{\overline{w'^3}}{\rho_s}\frac{\partial\rho_s\overline{w'^2}}{\partial z} - 3\overline{w'^3}\frac{\partial\bar{w}}{\partial z} + \frac{3g}{\theta_{vs}}\overline{w'^2\theta'_v} \\ &+ C_{15}K_m\left(\frac{g}{\theta_{vs}}\frac{\partial\overline{w'\theta'_v}}{\partial z} - \left(\frac{\partial\overline{u'v'}}{\partial z}\frac{\partial\bar{u}}{\partial z} + \frac{\partial\overline{u'v'}}{\partial z}\frac{\partial\bar{v}}{\partial z}\right)\right) \\ &- \frac{C_8}{\tau}\left(C_{8b}Skw^4+1\right)\overline{w'^3} - C_{11sk}\left(3\overline{w'^3}\frac{\partial\bar{w}}{\partial z} + \frac{3g}{\theta_{vs}}\overline{w'^2\theta'_v}\right) \\ &+ \frac{\partial\left[\left(K_w+\nu\right)\frac{\partial\overline{w'^3}}{\partial z}\right]}{\partial z}\end{aligned} \tag{10}$$

*C8* controls the magnitude of the Newtonian damping term ($-\frac{C_8}{\tau}\overline{w'^3}$), which is also affected by the dissipation time scale $\tau$. The Newtonian damping term represents the blocking effects caused by the stable stratification, because the dissipation time scale $\tau$ is small in stable layers. Thus, the Newtonian damping term


© 2014. The Authors.

J_ID: JAME Customer A_ID: JAME20101 Cadmus Art: JAME20101 Ed. Ref. No.: - Date: 15-July-14 Stage: Page: 16



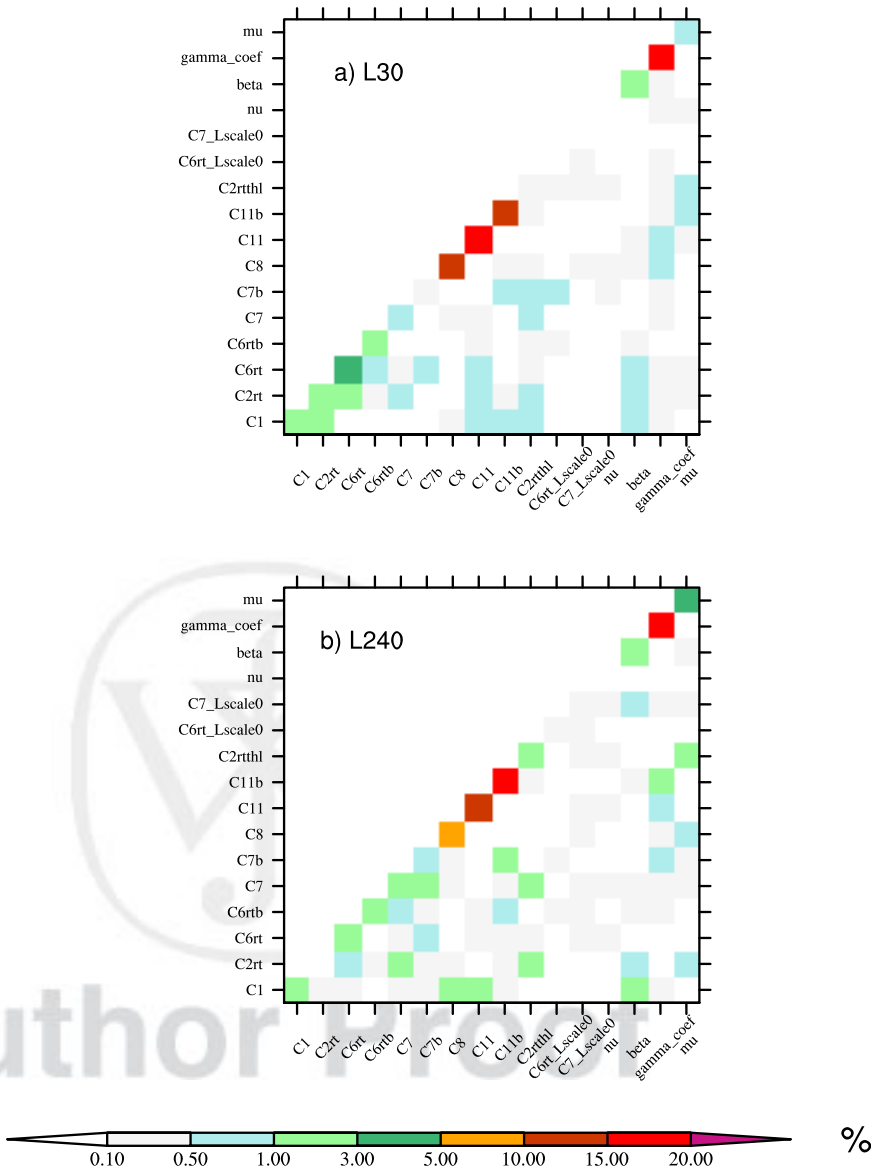


**Figure 10.** Relative contributions (percentage, shading) of interactions of tunable parameters to the variations of total cloud fraction estimated by the GLM in BOMEX. (a) At low vertical resolution (30 layers, L30) with $R^2$ of 0.97 (0.77 from individual terms); (b) at high vertical resolution (240 layers, L240) with $R^2$ of 0.94 (0.7 from individual terms).

with its peak usually locates near the stably stratified layer and damps the $\overline{w'^3}$ and skewness of vertical velocity. Large *C8* means a strong Newtonian damping that restricts $\overline{w'^3}$ and then the shallow convection.

The C11 skewness function ($C_{11sk}$) controls the pressure term ($-C_{11sk}(3\overline{w'^3}\frac{\partial \overline{w}}{\partial z} + \frac{3g}{\theta_{vs}}\overline{w'^2\theta'_v})$), in which the $\frac{\partial \overline{w}}{\partial z}$ term is negligible and the buoyancy-damping term with $\frac{3g}{\theta_{vs}}\overline{w'^2\theta'_v}$ dominates. In a conditionally unstable layer, the positive buoyancy fluxes are mainly driven by the surface heating flux and latent heating release from condensation [*Moeng and Rotunno*, 1990]. The positive buoyancy results in a positive skewness of vertical velocity fields associated with the conditional unstable layer. Thus, the pressure term (especially buoyancy-damping term) with its peak located in the conditional unstable layer mainly acts as a sink of the $\overline{w'^3}$ by weakening the conditional instability and consuming the initial buoyancy. It means stronger C11 skewness function produces stronger dissipation of the conditional instability. Those are favorable for reducing the $\overline{w'^3}$ in conditional unstable layers.

Similar to the C6 skewness function, the C11 skewness function ($C_{11sk}$) is defined as

 © 2014. The Authors. 

ID: kandasamy.d Time: 18:43 I Path: N:/3b2/JAME/Vol00000/140037/APPFile/JW-JAME140037

AGU Journal of Advances in Modeling Earth Systems 10.1002/2014MS000315

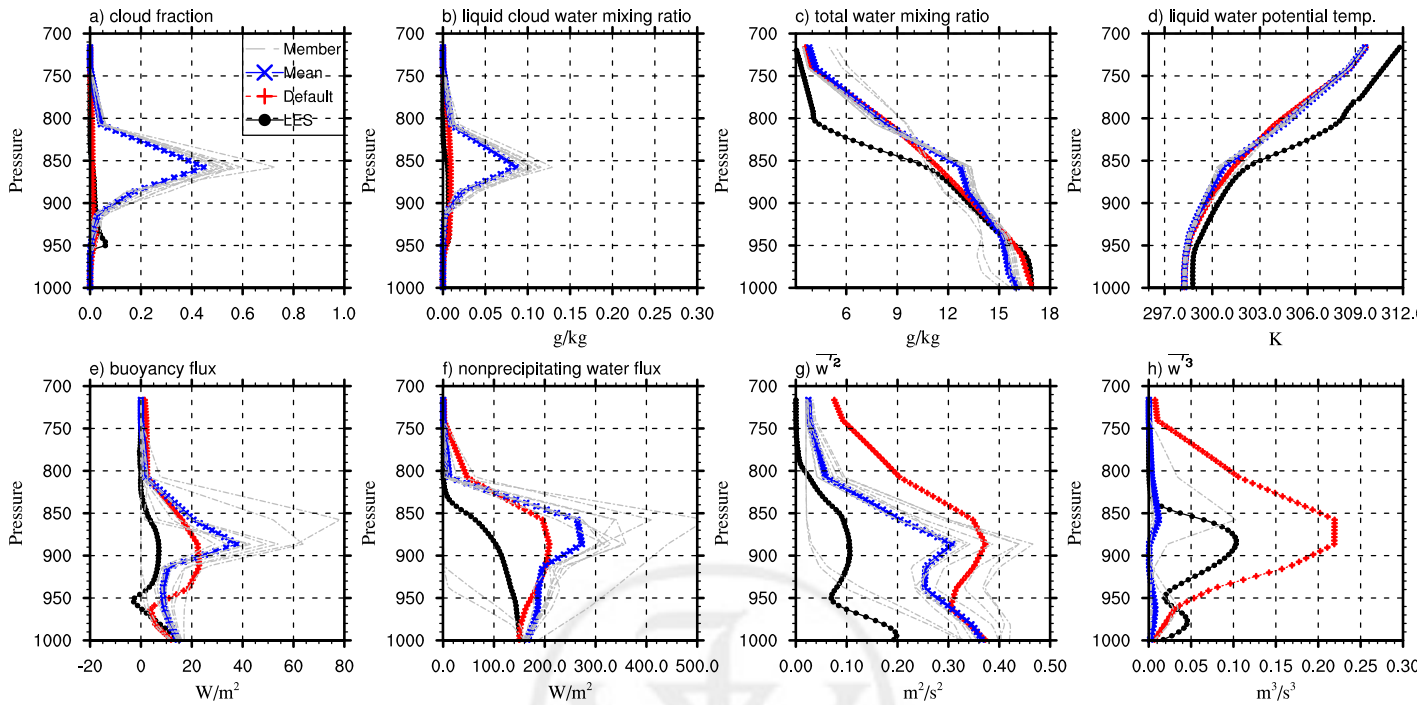


**Figure 11.** Mean vertical profiles of top 10 poor performance samples for the BOMEX case at low vertical resolution (30 layers), averaged over hours 5–6: (a) cloud fraction, (b) liquid cloud water mixing ratio (g/kg), (c) total water mixing ratio (g/kg), (d) liquid water potential temperature (K), (e) buoyancy flux (W/m$^2$), (f) total nonprecipitating water flux (W/m$^2$), (g) variance of vertical velocity ($\overline{w'^2}$, m$^2$/s$^2$), and (h) third-order moment of vertical velocity ($\overline{w'^3}$, m$^3$/s$^3$). The gray lines represent the individual samples (10), and the blue lines show average of those samples. The red lines indicate the LES results. The black lines indicate the profiles with the default parameter values.

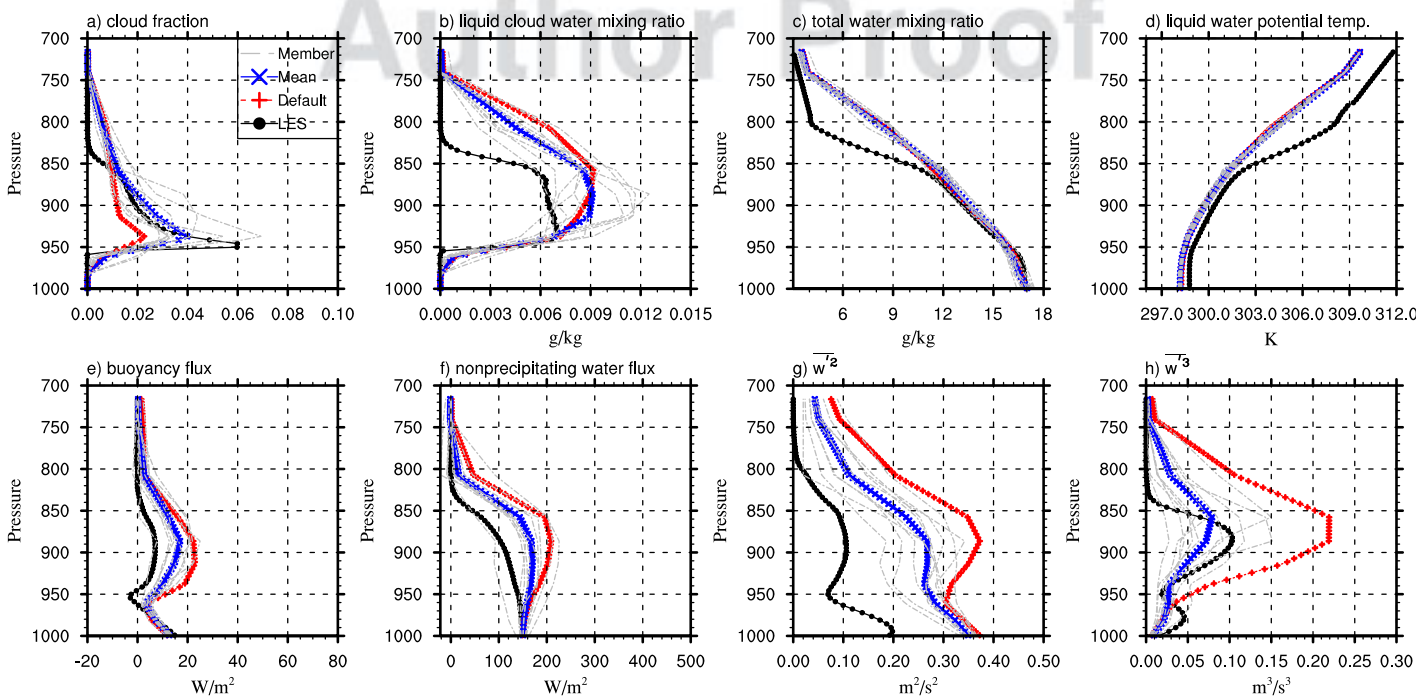


**Figure 12.** Same as Figure 11, but for top 10 good performance samples.


© 2014. The Authors.

AGU Journal of Advances in Modeling Earth Systems 10.1002/2014MS000315

$$C_{11sk} = C_{11b} + (C_{11} - C_{11b}) e^{-0.5 \times \left(\frac{Skw}{C_{11c}}\right)^2} \tag{11}$$

where the *C11*, *C11b*, and *C11c* are low skewness, large skewness, and degree of slope of C11 skewness function, respectively. *C11* and *C11b* are included in the 16-parameter experiments (Table 1), while *C11c* is included in the 35-parameter experiments (see the Table A1 and Appendix B).

When shallow convection develops, the *Skw* (equation (6)) is large in cumulus layer and therefore $C_{11sk}$ is closer to the large limit of skewness *C11b* than to *C11*. In this case, the second term in the right hand side of equation (11) becomes less important. This also helps to explain why *C11c* and *skw_denom_coef* (see equation (6)) contribute little to the total variance of cloud fraction when they are included in the 35-parameter experiments (see discussions in section 4.1).

$\gamma$, one of the largest contributors in both shallow convection and stratocumulus, has broad effects in CLUBB. It controls the width of the individual Gaussians in the PDF of vertical velocity directly [*Larson and Golaz*, 2005]:

$$\tilde{\sigma}_w^2 = \gamma \left[1 - \max\left(c_{w\theta_l}^2, c_{wq_t}^2\right)\right] \tag{12}$$

where $c_{w\theta_l}$ and $c_{wq_t}$ are the correlations of vertical velocity with liquid potential temperature and total water content, respectively.

$\gamma$ further indirectly determines the weight of the first Gaussian in the PDF (*mixt*), which is defined as [*Larson and Golaz*, 2005]

$$\text{mixt} = \frac{1}{2} \cdot \left[1 - \sqrt{\frac{\widehat{\text{Skw}}^2}{4 + \widehat{\text{Skw}}^2}}\right] \tag{13}$$

where $\widehat{Skw} = \frac{Skw}{\left(1 - \tilde{\sigma}_w^2\right)^{1.5}}$ represents normalized skewness. Large $\gamma$ tends to result in a small *mixt* and to shift the PDF towards the second Gaussian. This makes the shape of the PDF more suitable for cumulus. On the other hand, small $\gamma$ makes the PDF more suitable for stratocumulus. Therefore, a large $\gamma$ tends to widen PDF shape and amplify the turbulence transports and the buoyancy term $\frac{3g}{\theta_{vs}} \overline{w'^2\theta'_v}$ in equation (10), and vice versa. These two terms are source terms of $\overline{w'^3}$, and especially the buoyancy term is the leading source term to $\overline{w'^3}$, making $\gamma$ also an indirect amplifier to $\overline{w'^3}$. For example, $\gamma$ is usually lower than the default value with a mean value of just 0.2 in the samples with the worst 10 performance scores. The high-order terms $\overline{w'^2 q_t}$, $\overline{w'^2\theta_l}$, $\overline{w'^2\theta'_v}$, and $\overline{w'^4}$, which are associated with $\overline{w'^3}$, are consequently weak (Figure 13). Such a tight coupling between $\gamma$ and $\overline{w'^3}$ is the cause of cumulus preference for a larger value of $\gamma$.

It is notable that the choice of vertical resolution does not have a large impact on the sensitive parameters in shallow cumulus, including RICO and BOMEX. The reason is that the boundary layer is deeper and the inversion is much weaker, compared with the stratocumulus-topped boundary layer case examined in section 3.1. The inversion is too weak to redistribute the eddy kinetic energy horizontally and to cause a sharp vertical gradient in convective boundary layer. The vertical gradients of the eddy length and dissipation time at upper portion of the convective boundary layer are not as sharp as they at the top of the stratocumulus-topped boundary layer (not shown) and therefore are less sensitive to vertical resolution. Therefore, the influential parameters in shallow convection are not determined by the vertical resolution.

## 4. Discussion

### 4.1. Dependence on the Number of Tunable Parameters

Our results in section 3 are based on the 16-parameter experiments and show that the parameters related to Newtonian and buoyancy-damping terms of total water flux are the most influential parameters for stratocumulus, while those related to skewness of vertical velocity are the most influential parameters for shallow cumulus. Here we examine how the uncertain range of cloud response and their sensitive parameters may be different when different numbers of tunable parameters are chosen. Our results show that the most


© 2014. The Authors.

AGU Journal of Advances in Modeling Earth Systems 10.1002/2014MS000315

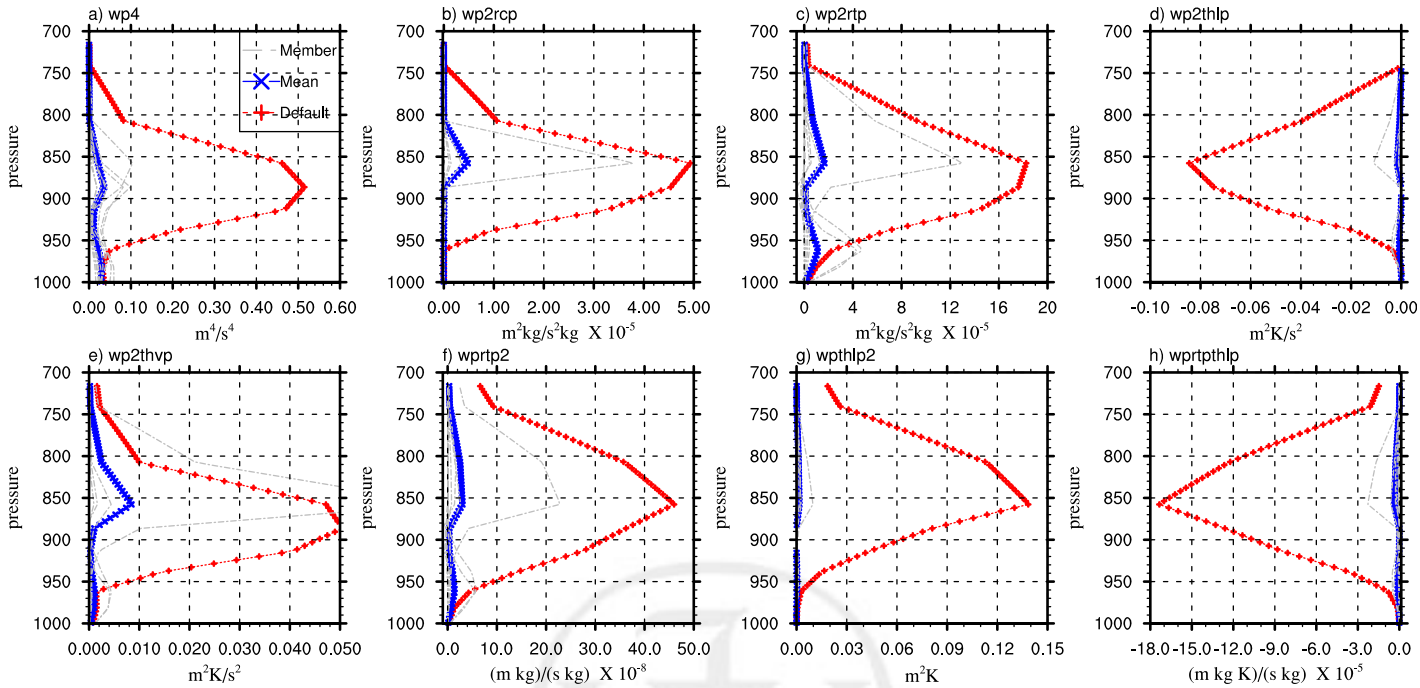


**Figure 13.** Mean vertical profiles of high-order PDF closure terms of top 10 poor performance samples for the BOMEX case at low resolution, averaged over hours 5–6: (a) $\overline{w'^4}$, (b) $\overline{w'^2q'_c}$, (c) $\overline{w'^2q'_t}$, (d) $\overline{w'^2\theta'_l}$, (e) $\overline{w'^2\theta'_v}$, (f) $\overline{w'q'^2_t}$, (g) $\overline{w'\theta'^2_l}$, and (h) $\overline{w'q'_t\theta'_l}$. The gray lines represent the individual samples (10), and the blue lines show average of those samples. The black lines indicate the profiles with the default parameter values.

influential parameters are similar when we reduce the number of tunable parameters from 35 to 16. The relative contributions of individual parameters from the full set 35-parameter SA are shown in Figure 14 (see the discussion in section 2.3.1 for the choice of parameters, Table A1 for the list of parameters and Figure B1 for cloud fraction variations with individual parameters). It shows that the parameters related to skewness of vertical velocity, including C8, C11, C11b, and $\gamma$, are still the most influential parameters in shallow convections and those related to Newtonian and buoyancy-damping terms of total water flux are still the largest contributors to the total variance of stratocumulus, similar with the 16-parameter SA (comparing Figure 14a with Figure 9). The difference is that the $R^2$ of individual parameters is smaller in the 35-parameter SA than those in the 16-parameter SA, because the 35-parameter SA generates more interaction terms (595 of 630) that partly reduce the contributions of individual parameters.

For the 35-parameter and 16-parameter SA, it includes those parameters that were introduced in *Golaz et al.* [2007] to produce skewness-dependent coefficients of pressure terms in the predictive moisture and heat fluxes equations (equations (7) and (8)) in order to better distinguish stratocumulus and shallow cumulus (those *sk* coefficients discussed in section 3). In another SA analysis with 29 parameters, we remove the skewness-dependence of the coefficients in scalar flux equations in the 35-parameter experiments by setting high skewness coefficients to the low skewness coefficients (C6rt = C6rtb, C6thl = C6thlb, and C7 = C7b; see Table A1 for the list of parameters), while the skewness-dependence of the coefficients used in the $\overline{w'^3}$ equation is kept (e.g., C11 and C8). The goal is to investigate how the skewness-dependence of the coefficients in scalar fluxes equations affect the relative contributions of individual parameters to the variance of simulated cloud properties.

For stratocumulus at low resolution, parameters related to the moisture and heat flux equations (C6rt and C7) play a more prominent role in the 29-parameter SA than in the 35-parameter SA while contributions from those related to the skewness of vertical velocity are further diminished (Figure 14b) (see Figure A2 for cloud fraction variations with individual parameters). This might be expected, as the moisture and heat fluxes are critical for simulating stratocumulus (see discussions in section 3), and decoupling C6sk and C7sk from the skewness of vertical velocity enhance the roles of these two parameters. For stratocumulus at high resolution, the differences between the 29-parameter SA and 35-parameter SA are less distinguishable. This might suggest that at high resolution, the boundary layer structure is better simulated and the skewness of

 © 2014. The Authors. 

AGU Journal of Advances in Modeling Earth Systems 10.1002/2014MS000315

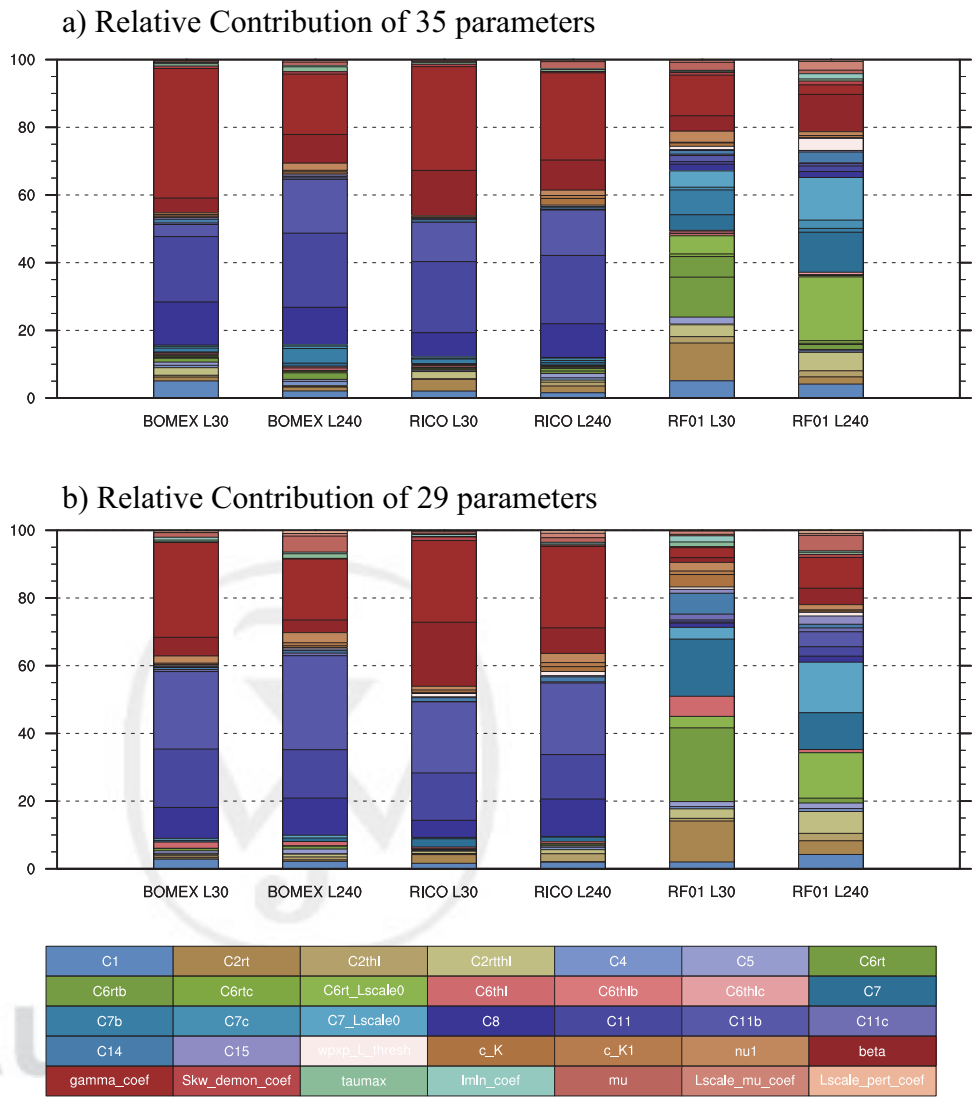


**Figure 14.** Same as Figure 9, but for (a) the 35-parameter experiments and (b) the 29-parameter experiments.

vertical velocity is generally small. Therefore, dropping the dependence of C6sk and C7sk on *Skw* makes little differences. For shallow cumulus, the contributions from C6sk and C7sk are further reduced in the 29-parameter SA compared to the 35-paramter SA. Another noticeable difference is that C11b plays a more prominent role while C11 is less important. It is still not clear why this is the case.

### 4.2. Implication for Other High-Order Parameterizations

As we discussed in sections 1 and 2, many CLUBB tunable parameters examined here are also commonly used in some other high-order closure parameterizations, especially those related to the pressure terms. The use of pressure terms, which show large contributions in CLUBB, trace back to *Rotta* [1951], *André et al.* [1978], and *Bougeault* [1981], and are continually or partly used in current high-order parameterizations. In the scheme of *Lappen and Randall* [2001], $-C\frac{\sqrt{e}}{Lscale}\overline{w'x'}$ represents the unified format of Newtonian damping, where x can be $\overline{w'}$, $\overline{w'^2}$, $q_t$ and $\theta_l$. Thus, parameter $C$ refers to $C_4$, $C_{6rt}$, $C_{6thl}$, and $C_8$ in flux equations used in CLUBB. *Cheng et al.* [2005] propose a third- and fourth-order moments scheme. In their scheme, $-4C_2\frac{\overline{\theta_l'^2}}{\tau}$, $-\frac{2C_4}{\tau}\left(\overline{w'^2}-\frac{1}{3}\bar{e}\right)$, $-\frac{2C_6}{\tau}\overline{w'\theta_l'}$ and $-\frac{2C_8}{\tau}\overline{w'^3}$ represent the Newtonian damping in equations of $\overline{\theta_l'^2}$, $\overline{w'^2}$, $\overline{w'\theta_l'}$ and $\overline{w'^3}$, respectively. Moreover, the buoyancy-damping terms are shown as $-C_5\frac{4g\alpha}{3}\overline{w\theta}$, $-C_7g\alpha\overline{\theta^2}$, $-3(1-C_{11})g\alpha\overline{w^2\theta}$ in $\overline{w^2}$, $\overline{w\theta}$, and $\overline{w'^3}$ equations, respectively, where $\alpha$ is the coefficient of thermal


© 2014. The Authors.

AGU Journal of Advances in Modeling Earth Systems 10.1002/2014MS000315

**Table 2.** Values of Key CLUBB Parameters that Produce the Best Joint Performance Score for DYCOMS-II RF01 (Stratocumulus) and BOMEX (Shallow Cumulus)

| Parameter | C6rt | C6rtb | C7 | C7b | $\gamma$ | C11 | C11b | C8 |
|---|---|---|---|---|---|---|---|---|
| Default | 4.00 | 6.00 | 0.50 | ~~0.35~~ | 0.32 | 0.80 | 0.65 | 3.00 |
| Best | 2.84 | 7.01 | 0.42 | 0.71 | 0.22 | 0.38 | 0.48 | 4.50 |

expansion. Although these terms ~~have~~ somewhat different ~~form~~ CLUBB, they are similar to CLUBB in essence. Therefore, the sensitivity analysis of simulated cloud fields to the influential parameters in CLUBB can also be applicable for these other high-order closure parameterizations and further helps to guide their improvement.

### 4.3. Model Parameters in the "Best" Performance Simulations

Based on the "joint" performance scores of the BOMEX and DYCOMS-II RF01 experiments at low-resolution with the 35 tunable parameters, we identify a set of parameters that produce the best joint performance score. The joint performance score is defined as the product of the performance scores from BOMEX and DYCOMS-II RF01, which is described in section 2.3.4.

Table 2 shows the values of the key parameters used in the "best" simulations. This best parameter set agrees well with the SA in section 3 and works for both stratocumulus and shallow cumulus. First, the smaller values of *C11b*, *C11*, and *C8* reduce the pressure damping terms resulting in a larger skewness of vertical velocity $\overline{w'^3}$ and improve cumulus simulations. Second, the smaller values of *C6rt* and *C7* help to enhance water flux for stratocumulus. The contributions from the other parameters are small (varying these parameters has small impacts on the results). As shown in Figure 15, CLUBB with this set of key parameters performs well in all three cases. Note that the set of parameters with the best performance score may not be the optimal set, as the SA framework applied in this study is most suitable for sensitive studies, not for calibration. A more rigid calibration of the CLUBB parameters will require other frameworks, such as Multiple Very Fast Simulated Annealing applied in *Yang et al.* [2012] which samples the parameters based on a performance score so that the algorithm progressively moved toward the parameter region to minimize model errors. Nevertheless, the selected best set of parameters confirms the conclusions of our SAs and helps us to better understand the physical processes of CLUBB.

## 5. Summary

In this study, we have applied a sensitivity analysis (SA) framework to analyze the variation of simulated stratocumulus and shallow cumulus properties due to perturbations in Cloud Layers Unified by Binormals (CLUBB) tunable parameters in the state-of-the-art single-column version of the ~~NCAR~~ Community Atmosphere Model Version 5 (SCAM5). The analysis of stratocumulus and cumulus cases reveals a large range in cloud property response to perturbations of CLUBB tunable parameters. For example, total cloud fraction in the stratocumulus case ranges from 0% to 100%. Such large ranges indicate the urgency of quantifying and understanding the uncertainty of CLUBB simulations to its tunable parameters.

The Generalized Linear Model (GLM) is used to emulate CLUBB-simulated variations of stratocumulus and shallow cumulus at two different vertical resolutions: 30 and 240 layers. The results show that the variation in stratocumulus simulations is dominated by the moisture turbulence within the assigned parameter ranges. The parameters related to Newtonian and buoyancy-damping terms in the total water mixing ratio flux predictive equation are found to have statistically significant impact on the cloud fraction of stratocumulus. The Newtonian damping term, which is dominated by *C6rt* through the C6 skewness function, blocks vertical mixing in the cloud layer. The buoyancy-damping term, which is controlled by *C7* through C7 skewness function, influences the strength of decoupling at cloud base and entrainment in the cloud layer. *C6rt* and *C7* are two of the most effective tuning parameters for the stratocumulus at low resolution of SCAM5.

The parameters associated with the skewness of vertical velocity are the most effective tuning parameters for shallow convection, such as $\gamma$, *C11b*, *C11*, and *C8*. The additional buoyancy-damping term associated with conditional instability, which is controlled by *C11* and *C11b*, restricts and consumes positive buoyancy fluxes. The Newtonian damping term related to *C8* blocks updrafts of convection, which represent the effects of stable stratification. The perturbation of $\gamma$ not only significantly influences the width of individual


© 2014. The Authors.


ID: kandasamy.d Time: 18:43 I Path: N:/3b2/JAME/Vol00000/140037/APPFile/JW-JAME140037

AGU Journal of Advances in Modeling Earth Systems 10.1002/2014MS000315

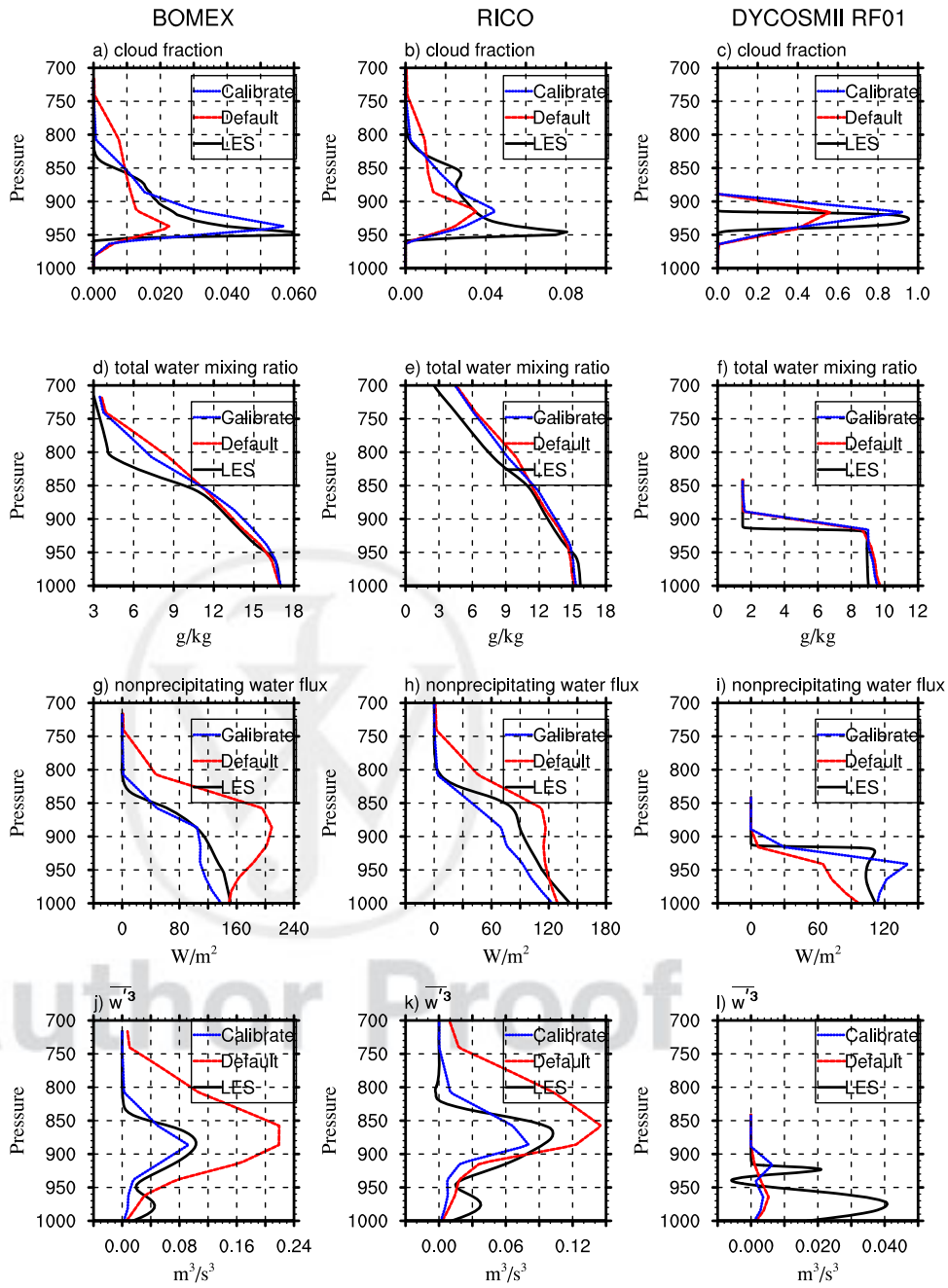


**Figure 15.** Mean vertical profiles of (a–c) cloud fraction, (d–f) total water mixing ratio (g/kg), (g–i) total nonprecipitating water flux (W/m$^2$), and (j–l) buoyancy flux (W/m$^2$) in two shallow convection cases (BOMEX averaged over hours 5–6 and RICO averaged over hours 7–8) and one stratocumulus case (DYCOMSII RF01 averaged over hours 3–4). The black lines indicate the LES. The red lines indicate the profiles from the default parameter values. The blue lines represent the profiles with the best joint performance score.

Gaussians in the PDF and normalized skewness of vertical velocity but also substantially affects the high-order terms by changing the PDF shape.

It is interesting that the vertical resolution has a large impact on which parameters are most influential for stratocumulus clouds. The stratocumulus-covered boundary layer is usually shallow and occurs under a strong and sharp inversion, which causes large vertical gradients near boundary layer top. Thus, vertical resolution is critical in stratocumulus cases, as the eddy mixing length and eddy dissipation time are strongly dependent on the vertical resolution in stratocumulus. The additional Newtonian damping term, which was introduced in CLUBB to block gravity waves in stably stratified layer and enhance inversions,


© 2014. The Authors.

AGU Journal of Advances in Modeling Earth Systems 10.1002/2014MS000315

becomes more important at high vertical resolution. Thus, its controller *C6rt_Lscale0* replaces *C6rt* as the key parameter to C6 skewness function and the stratocumulus. Unlike DYCOMSII RF01, the vertical resolution does not have a large impact on the sensitivity of parameters in BOMEX and RICO shallow convection cases (Figure 9). Because the convective boundary layer is deeper and occurs under a weak inversion, the turbulence kinetic energy extends vertically and allows a longer eddy dissipation time (or length) and smaller vertical gradient, which is less dependent on the vertical resolution.

Our results showed that the influential parameters in the 35-parameter experiments and 16-parameter experiments are essentially the same, while removing the skewness-dependence of some coefficients in the predictive moisture and heat fluxes equations that were originally introduced to better distinguish stratocumulus and shallow cumulus [*Golaz et al.*, 2007] can produce somewhat different results (Figure 14).

A set of parameters that produce the best joint performance score for both stratocumulus and shallow cumulus cases are identified from the 35-parameter experiments. This set of parameters confirms the conclusions of our SA, and our preliminary test shows that the global CAM5 run with this best set of parameters produces a credible global simulation with enhanced low cloud fraction from 41% to 49% with little change in middle and high cloud fraction (not shown).

Given that CLUBB shares common parameters with many other high-order closure parameterizations, the sensitivity analysis presented in this study can also be applicable to other high-order closure parameterizations and further helps to guide their improvement in the future.

Our results suggest that a small subset of 35 CLUBB tunable parameters can explain most of the variance in simulated cloud fields of SCAM5 with CLUBB. This study therefore helps us to reduce the number of tunable parameters for our ongoing sensitivity and calibration study of global simulations.

## Appendix A: CLUBB Equations and Tunable Parameters

For the convenience of the reader, here we list CLUBB's prognostic equations that contain tunable parameters:

$$\begin{aligned}\frac{\partial \overline{w'^2}}{\partial t} &= -\bar{w}\frac{\partial \overline{w'^2}}{\partial z} - \frac{1}{\rho_s}\frac{\partial \rho_s \overline{w'^3}}{\partial z} - 2\overline{w'^2}\frac{\partial \bar{w}}{\partial z} + \frac{2g}{\theta_{vs}}\overline{w'\theta'_v} - \frac{C_4}{\tau}\left(\overline{w'^2} - \frac{2}{3}\bar{e}\right) \\ &\quad - C_5\left(-2\overline{w'^2}\frac{\partial \bar{w}}{\partial z} + \frac{2g}{\theta_{vs}}\overline{w\theta'_v}\right) + \frac{2}{3}C_5\left(\frac{g}{\theta_{vs}}\overline{w\theta'_v} - \overline{u'w'}\frac{\partial \bar{u}}{\partial z} - \overline{v'w'}\frac{\partial \bar{v}}{\partial z}\right) \\ &\quad - \frac{C_1}{\tau}\left(\overline{w'^2} - w|^2_{tol}\right) + \frac{\partial\left[(K_w+\nu)\frac{\partial \overline{w'^2}}{\partial z}\right]}{\partial z} + \left.\frac{\partial \overline{w'^2}}{\partial t}\right|_{pd} + \left.\frac{\partial \overline{w'^2}}{\partial t}\right|_{cl}\end{aligned} \tag{A1}$$

$$\begin{aligned}\frac{\partial \overline{q'^2_t}}{\partial t} &= -\bar{w}\frac{\partial \overline{q'^2_t}}{\partial z} - \frac{1}{\rho_s}\frac{\partial \rho_s \overline{w'q'^2_t}}{\partial z} - 2\overline{w'q'_t}\frac{\partial \bar{w}}{\partial z} - \frac{C_{2rt}}{\tau}\left(\overline{q'^2_t} - q_t|^2_{tol}\right) + \frac{\partial\left[(K_w+\nu)\frac{\partial \overline{q'^2_t}}{\partial z}\right]}{\partial z} \\ &\quad + \left.\frac{\partial \overline{q'^2_t}}{\partial t}\right|_{pd} + \left.\frac{\partial \overline{q'^2_t}}{\partial t}\right|_{cl}\end{aligned} \tag{A2}$$

$$\begin{aligned}\frac{\partial \overline{\theta'^2_l}}{\partial t} &= -\bar{w}\frac{\partial \overline{\theta'^2_l}}{\partial z} - \frac{1}{\rho_s}\frac{\partial \rho_s \overline{w'\theta'^2_l}}{\partial z} - 2\overline{w'\theta'_l}\frac{\partial \bar{w}}{\partial z} - \frac{C_{2thl}}{\tau}\left(\overline{\theta'^2_l} - \theta_l|^2_{tol}\right) + \frac{\partial\left[(K_w+\nu)\frac{\partial \overline{\theta'^2_l}}{\partial z}\right]}{\partial z} \\ &\quad + \left.\frac{\partial \overline{\theta'^2_l}}{\partial t}\right|_{pd} + \left.\frac{\partial \overline{\theta'^2_l}}{\partial t}\right|_{cl}\end{aligned} \tag{A3}$$


© 2014. The Authors.


ID: kandasamy.d Time: 18:43 I Path: N:/3b2/JAME/Vol00000/140037/APPFile/JW-JAME140037

AGU Journal of Advances in Modeling Earth Systems 10.1002/2014MS000315

$$\frac{\partial \overline{q'_t\theta'_l}}{\partial t} = -\bar{w}\frac{\partial \overline{q'_t\theta'_l}}{\partial z} - \frac{1}{\rho_s}\frac{\partial \rho_s \overline{w'q'_t\theta'_l}}{\partial z} - \overline{w'q'_t}\frac{\partial \bar{\theta}_l}{\partial z} - \overline{w'\theta'_l}\frac{\partial \bar{q}_t}{\partial z} - \frac{C_{2rtthl}}{\tau}\overline{q'_t\theta'_l} + \frac{\partial\left[(K_w+\nu)\frac{\partial \overline{q'_t\theta'_l}}{\partial z}\right]}{\partial z} + \left.\frac{\partial \overline{q'_t\theta'_l}}{\partial t}\right|_{cl} \tag{A4}$$

$$\frac{\partial \overline{w'q'_t}}{\partial t} = -\bar{w}\frac{\partial \overline{w'q'_t}}{\partial z} - \frac{1}{\rho_s}\frac{\partial \rho_s \overline{w'^2q'_t}}{\partial z} - \overline{w'^2}\frac{\partial \bar{q}_t}{\partial z} - \overline{w'q'_t}\frac{\partial \bar{w}}{\partial z} + \frac{g}{\theta_{vs}}\overline{q'_t\theta'_v} - \frac{C_{6sk}}{\tau}\overline{w'q'_t} + C_{7sk}\overline{w'q'_t}\frac{\partial \bar{w}}{\partial z} - C_{7sk}\frac{g}{\theta_{vs}}\overline{q'_t\theta'_v} + \frac{\partial\left[(K_w+\nu)\frac{\partial \overline{w'q'_t}}{\partial z}\right]}{\partial z} + \left.\frac{\partial \overline{w'q'_t}}{\partial t}\right|_{sicl} + \left.\frac{\partial \overline{w'q'_t}}{\partial t}\right|_{cl} + \left.\frac{\partial \overline{w'q'_t}}{\partial t}\right|_{mfl} \tag{A5}$$

$$\frac{\partial \overline{w'\theta'_l}}{\partial t} = -\bar{w}\frac{\partial \overline{w'\theta'_l}}{\partial z} - \frac{1}{\rho_s}\frac{\partial \rho_s \overline{w'^2\theta'_l}}{\partial z} - \overline{w'^2}\frac{\partial \bar{\theta}_l}{\partial z} - \overline{w'\theta'_l}\frac{\partial \bar{w}}{\partial z} + \frac{g}{\theta_{vs}}\overline{\theta'_l\theta'_v} - \frac{C_{6sk}}{\tau}\overline{w'\theta'_l} + C_{7sk}\overline{w'\theta'_l}\frac{\partial \bar{w}}{\partial z} - C_{7sk}\frac{g}{\theta_{vs}}\overline{\theta'_l\theta'_v} + \frac{\partial\left[(K_w+\nu)\frac{\partial \overline{w'\theta'_l}}{\partial z}\right]}{\partial z} + \left.\frac{\partial \overline{w'\theta'_l}}{\partial t}\right|_{sicl} + \left.\frac{\partial \overline{w'\theta'_l}}{\partial t}\right|_{cl} + \left.\frac{\partial \overline{w'\theta'_l}}{\partial t}\right|_{mfl} \tag{A6}$$

$$\frac{\partial \overline{w'^3}}{\partial t} = -\bar{w}\frac{\partial \overline{w'^3}}{\partial z} - \frac{1}{\rho_s}\frac{\partial \overline{w'^4}}{\partial z} + 3\frac{\overline{w'^3}}{\rho_s}\frac{\partial \rho_s \overline{w'^2}}{\partial z} - 3\overline{w'^3}\frac{\partial \bar{w}}{\partial z} + \frac{3g}{\theta_{vs}}\overline{w'^2\theta'_v} + C_{15}K_m\left(\frac{g}{\theta_{vs}}\frac{\partial \overline{w'\theta'_v}}{\partial z} - \left(\frac{\partial \overline{u'v'}}{\partial z}\frac{\partial \bar{u}}{\partial z} + \frac{\partial \overline{u'v'}}{\partial z}\frac{\partial \bar{v}}{\partial z}\right)\right) - \frac{C_8}{\tau}\left(C_{8b}Skw^4+1\right)\overline{w'^3} - C_{11sk}\left(3\overline{w'^3}\frac{\partial \bar{w}}{\partial z} + \frac{3g}{\theta_{vs}}\overline{w'^2\theta'_v}\right) + \frac{\partial\left[(K_w+\nu)\frac{\partial \overline{w'^3}}{\partial z}\right]}{\partial z} \tag{A7}$$

$$\frac{\partial \overline{u'^2}}{\partial t} = -\bar{w}\frac{\partial \overline{u'^2}}{\partial z} - \frac{1}{\rho_s}\frac{\partial \rho_s \overline{w'u'^2}}{\partial z} - (1-C_{5sk})2\overline{u'w'}\frac{\partial \bar{w}}{\partial z} - \frac{2}{3}\frac{C_{14sk}\bar{e}}{\tau} + \frac{2}{3}C_{5sk}\left(\frac{g}{\theta_{vs}}\overline{w\theta'_v} - \overline{u'w'}\frac{\partial \bar{u}}{\partial z} - \overline{v'w'}\frac{\partial \bar{v}}{\partial z}\right) - \frac{C_{4sk}}{\tau}\left(\overline{u'^2} - \frac{2}{3}\bar{e}\right) + \frac{\partial\left[(K_w+\nu)\frac{\partial \overline{u'^2}}{\partial z}\right]}{\partial z} + \left.\frac{\partial \overline{u'^2}}{\partial t}\right|_{pd} + \left.\frac{\partial \overline{u'^2}}{\partial t}\right|_{cl} \tag{A8}$$


© 2014. The Authors.


ID: kandasamy.d Time: 18:43 I Path: N:/3b2/JAME/Vol00000/140037/APPFile/JW-JAME140037

AGU Journal of Advances in Modeling Earth Systems 10.1002/2014MS000315

**Table A1.** CLUBB Parameters in the 35-Parameter Experiments[a]

| Tuning Parameter | Description | Default Value | Investigated Range |
|---|---|---|---|
| C1[b,c] | Low Skewness in C1 Skewness Function | 2.5 | 1.25–5 |
| C2rt[b,c] | Constant associated with $\overline{r'_t{}^2}$ dissipation | 1.0 | 0.5–2 |
| C2thl[c] | Constant associated with $\overline{\theta'_l{}^2}$ dissipation | 1.0 | 0.5–2 |
| C2rtthl[c] | Constant associated with $\overline{r'_t\theta'_l}$ dissipation | 1.0 | 0.5–2 |
| C4[c] | Return to isotropy term in $\overline{w'^2}$, $\overline{u'^2}$, $\overline{v'^2}$ | 5.2 | 2.6–10.4 |
| C5[c] | Constant in $\overline{w'^2}$ pressure term | 0.3 | 0.0–1.0 |
| C6rt[b,c] | Low Skewness in C6rt Skewness Function | 4.0 | 2.0–8.0 |
| C6rtb[b] | High Skewness in C6rt Skewness Function | 6.0 | 2.0–8.0 |
| C6rtc | Degree of Slope of C6rt Skewness Function | 0.5 | 0.25–1.75 |
| C6thl[c] | Low Skewness in C6thl Skewness Function | 4.0 | 2.0–8.0 |
| C6thlb | High Skewness in C6thl Skewness Function | 6.0 | 2.0–8.0 |
| C6thlc | Degree of Slope of C6thl Skewness Function | 0.5 | 0.25–1.75 |
| C7[b,c] | Low Skewness in C7 Skewness Function | 0.5 | 0.0–1.0 |
| C7b[b] | High Skewness in C7 Skewness Function | 0.8 | 0.0–1.0 |
| C7c | Degree of Slope of C7 Skewness Function | 0.5 | 0.0–1.0 |
| C8[b,c] | Coefficient in C8 Skewness Equation | 3.0 | 1.5–6.0 |
| C11[b,c] | Low Skewness in C11 Skewness Function | 0.8 | 0.0–1.0 |
| C11b[b,c] | High Skewness in C11 Skewness Function | 0.65 | 0.0–1.0 |
| C11c[c] | Degree of Slope of C11 Skewness Function | 0.5 | 0.25–1.75 |
| C14[c] | Constant applied to $\overline{u'^2}$ and $\overline{v'^2}$ | 1.0 | 0.5–2.0 |
| C15[c] | Constant applied to $\overline{w'^3}$ bp2 | 0.4 | 0.2–0.8 |
| C6_Lscale0[b,c] | Used to damp C6rt as a function of *Lscale* | 14.0 | 7.0–28.0 |
| C7_Lscale0[b,c] | Used to damp C7 as a function of *Lscale* | 0.85 | 0.425–1.7 |
| wpxp_L_thresh[c] | Lscale threshold for C6 and C7 coefficients | 60.0 | 30.0–120.0 |
| $c_k$[c] | Coefficient of Eddy Diffusion | 0.2 | 0.1–0.4 |
| $c_{k1}$[c] | Coefficient of individual Eddy Diffusion | 0.5 | 0.25–1.0 |
| $\nu$(nu)[b,c] | Background Coefficient of Eddy Diffusion | 20.0 | 10.0–40.0 |
| $\beta$(beta)[b,c] | Constant related to "plume" variance of $\overline{\theta'_l{}^2}$ and $\overline{r'_t{}^2}$ | 1.75 | 0.0–3.0 |
| $\gamma$(gamma_coef) [b,c] | Low Skewness in $\gamma$ coefficient Skewness Function | 0.32 | 0.0–0.83 |
| $\tau_{max}$(tau_max)[c] | Maximum allowable value of time scale $\tau$ | 3600 | 1800–7200 |
| lmin_coef[c] | Coefficient of the minimum allowable *Lscale* | 0.5 | 0.25–1.0 |
| $\mu$(mu)[b,c] | Parcel Entrainment Rate (Lscale) [1/m] | $1 \times 10^{-3}$ | $0.5–2.0 \times 10^{-3}$ |
| Lscale_[~~Errorhx00A0~~]$\mu$_coef[c] | Coefficient to perturb $\mu$ for an average calculation of Lscale | 2.0 | 1.0–4.0 |
| Lscale_pert_coef[c] | Coefficient to perturb $\bar{\theta}_l$ and $\bar{r}_t$ for an average calculation of Lscale | 0.1 | 0.05–0.2 |
| Skw_denom_coef[c] | Additional damping to skewness | 0.0 | 0–10 |

[a]Texts in brackets are the name in source code of CLUBB.
[b]Parameters used in the 16-parameter experiments.
[c]Parameters used in the 29-parameter experiments.


© 2014. The Authors.

AGU Journal of Advances in Modeling Earth Systems 10.1002/2014MS000315

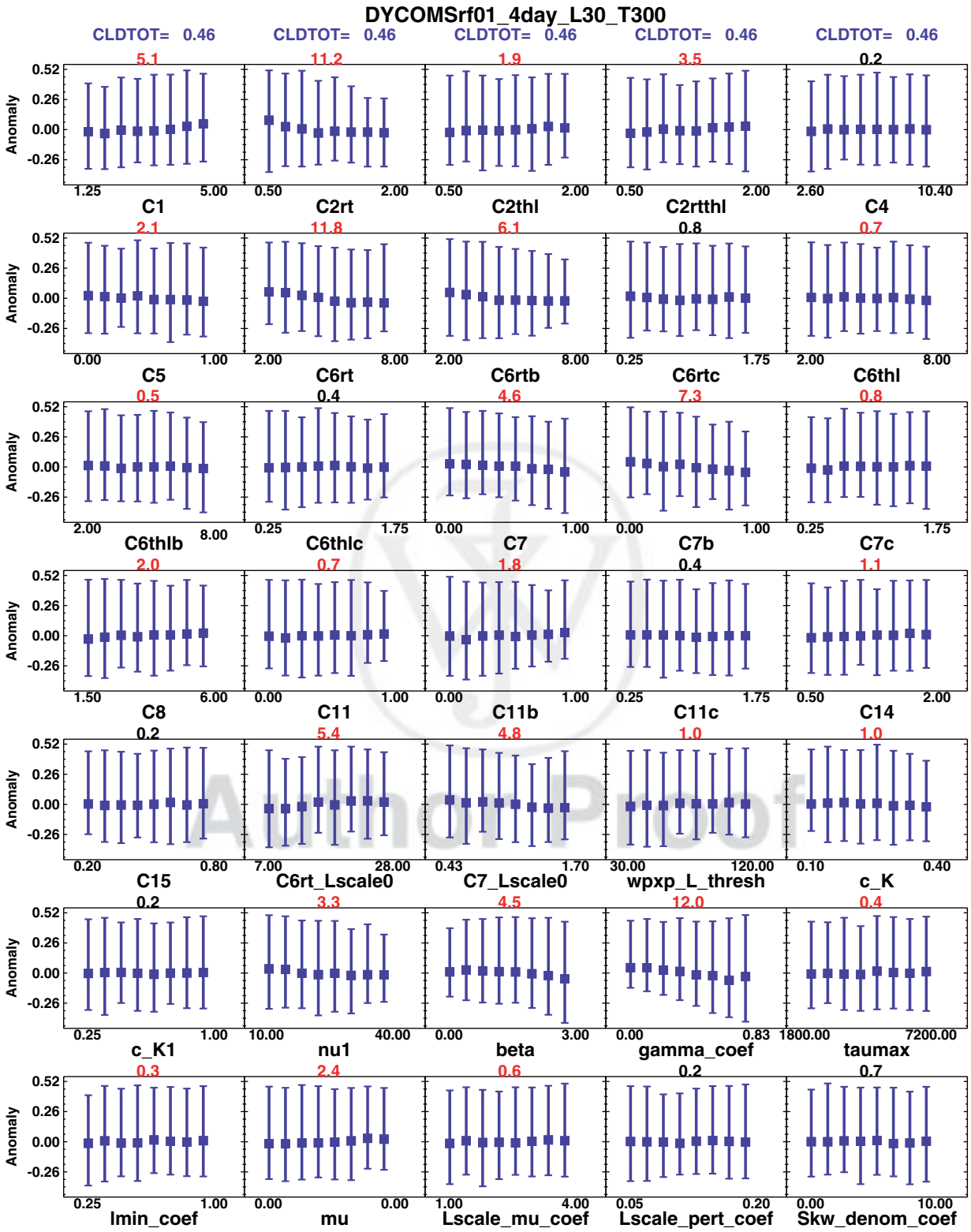


**Figure A1.** Anomalies of variation of total cloud fraction averaged over hours 3–4 in response to the perturbations of 35 parameters from the 4096 SCAM5-CLUBB DYCOMSII RF01 simulations. The vertical resolution of SCAM5-CLUBB is 30 layers (L30). The mean total cloud fraction of ~~256~~ simulations is shown as CLDTOT. The numbers above each plot box represent the relative contribution (percentage) of each input parameter perturbation to the overall cloud fraction variations. Red means the contribution with 95% statistic significance. The mean is denoted as boxes, while the vertical bars show the range of cloud fraction anomaly from tenth percentile (lower) to ninetieth percentile (upper).


© 2014. The Authors.

AGU Journal of Advances in Modeling Earth Systems 10.1002/2014MS000315

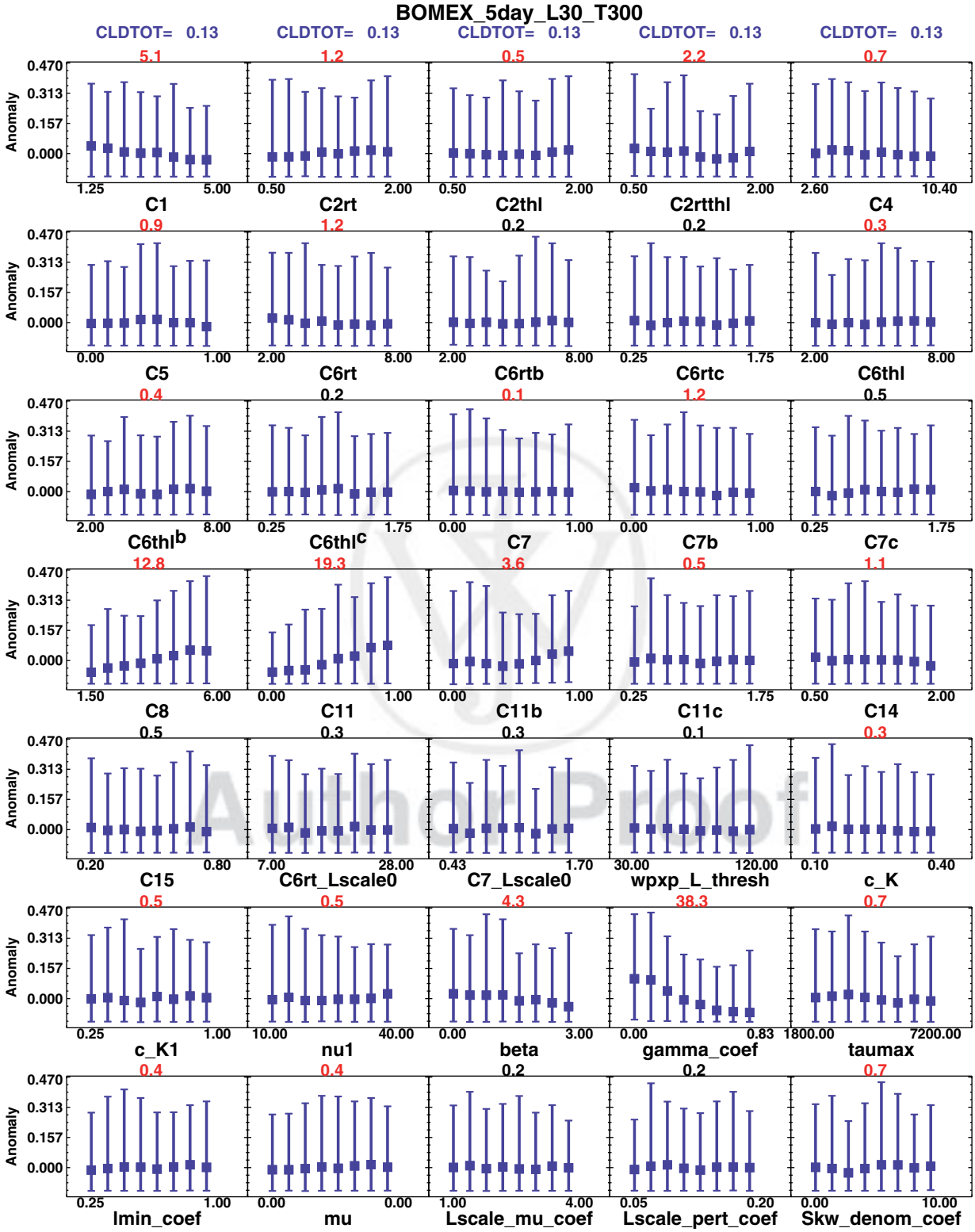


**Figure A2.** Same as Figure A1, except for BOMEX case.


© 2014. The Authors.

AGU Journal of Advances in Modeling Earth Systems 10.1002/2014MS000315

$$\frac{\partial \overline{v'^2}}{\partial t} = -\bar{w}\frac{\partial \overline{v'^2}}{\partial z} - \frac{1}{\rho_s}\frac{\partial \rho_s \overline{w'v'^2}}{\partial z} - (1-C_{5sk})2\overline{v'w'}\frac{\partial \bar{w}}{\partial z} - \frac{2}{3}\frac{C_{14sk}\bar{e}}{\tau}$$
$$+\frac{2}{3}C_{5sk}\left(\frac{g}{\theta_{vs}}\overline{w\theta'_v} - \overline{u'w'}\frac{\partial \bar{u}}{\partial z} - \overline{v'w'}\frac{\partial \bar{v}}{\partial z}\right) - \frac{C_{4sk}}{\tau}\left(\overline{v'^2} - \frac{2}{3}\bar{e}\right) \tag{A9}$$
$$+\frac{\partial\left[(K_w+\nu)\frac{\partial \overline{v'^2}}{\partial z}\right]}{\partial z} + \left.\frac{\partial \overline{v'^2}}{\partial t}\right|_{pd} + \left.\frac{\partial \overline{v'^2}}{\partial t}\right|_{cl}$$

where $\bar{u}$, $\bar{v}$, and $\bar{w}$ represent the grid-mean zonal, meridional, and vertical wind; $\bar{\theta}_l$ and $\bar{q}_t$ represent grid-mean liquid potential temperature and total water content; the second order terms $\overline{w'^2}$, $\overline{u'^2}$, $\overline{v'^2}$, $\overline{q'^2_t}$, $\overline{\theta'^2_l}$, $\overline{q'_t\theta'_l}$, $\overline{q'_tw'}$, and $\overline{\theta'_lw'}$ are variances and scalar terms; $\overline{w'^3}$ is the third-order moment of vertical velocity [*Golaz et al.*, 2002a, ~~2002b~~; *Larson and Golaz*, 2005; *Larson et al.*, 2012]. AQ6

Furthermore, $\theta_v$ is the virtual potential temperature; $\theta_{vs}$ is dry, static, base-state $\theta_v$. $\rho_s$ is dry, static, base-state density, which only changes with respect to altitude. $\tau$ represents the dissipation time scale and $\bar{e}$ means turbulence kinetic energy. $\theta_l|^2_{tol}$, $r_t|^2_{tol}$, and $w|^2_{tol}$ are the threshold values of variances $\overline{\theta'^2_l}$, $\overline{r'^2_t}$, and $\overline{w'^2}$.

The subscript *pd* denotes the rate of change due to the positive-definite hole-filling scheme, the subscript *sicl* is the rate of change due to the semi-implicit clipping scheme, the subscript *cl* is the rate of change due to completely explicit clipping, and the subscript *mfl* denotes adjustments from the monotonic flux limiter.

The subscript *sk* represents the skewness function of some of tunable parameters. Parameters used the 35-parameter experiments are included in Table A1. Some of the uncertain parameters have been used as tunable parameters in previous studies [e.g., *Golaz et al.*, 2007; *Bogenschutz et al.*, 2013; *Guo et al.*, 2014].

In above equations, *C1* controls the dissipation rate of the vertical velocity variance $\overline{w'^2}$ in equation (A1). The C2*thl*, C2*rt*, and C2*thlrt* control the dissipation rate of the vertical velocity variance $\overline{q'^2_t}$, $\overline{\theta'^2_l}$, and $\overline{q'_t\theta'_l}$, respectively, in equations (A2)–(A4). *C4* and *C5* appear in the parameterization of the pressure correlation term in $\overline{w'^2}$ equation in equation (A1).

C6 and C7 skewness functions appear in the parameterization of the pressure correlation term of scalar flux equations (equations (A5) and (A6)). When the eddy mixing length falls below the threshold that is defined by *wpxp_L_thresh*, the maximum value of C6 and C7 skewness functions will be controlled by *C6_Lscale0* and *C7_Lscale0*. Otherwise, C6 and C7 skewness functions are controlled by *C6rt*, *C6rtb*, *C6thl*, *C6thlb*, *C7*, and *C7b* (equations (A5) and (A6)).

*C8*, *C15*, and *C11x* ("x" represents a, b, and c) are part of Newtonian term and buoyancy-damping term in third-order moment vertical velocity $\overline{w'^3}$ equation (A7). C14 controls the dissipation rate of the vertical velocity variance $\overline{u'^2}$ and $\overline{v'^2}$. $c_k$, $c_{k1}$, and $\nu$ (nu) control the eddy diffusivity coefficients in equations of $\overline{w'^2}$, $\overline{u'^2}$, $\overline{v'^2}$, $\overline{q'^2_t}$, $\overline{\theta'^2_l}$, $\overline{q'_t\theta'_l}$, $\overline{q'_tw'}$, $\overline{\theta'_lw'}$, and $\overline{w'^3}$.

Other parameters do not directly appear in these equations, but they also play important roles in diagnosing eddy diffusion and high-order closures. $\beta$ and $\gamma$ are dimensionless parameters, which determine the shape of PDF function. For example, $\gamma$ is proportional to the normalized standard deviations ($\tilde{\sigma}^2_w$, equation (A10)) of each individual Gaussian and $\beta$ controls skewness of total water and liquid potential temperature [*Larson and Golaz*, 2005].

$$\tilde{\sigma}^2_w = \gamma\left[1-\max\left(c^2_{w\theta_l}, c^2_{wq_t}\right)\right] \tag{A10}$$

$$Skw = \frac{\overline{w'^3}}{\left(\overline{w'^2} + Skw_demon_coef \times \overline{w'^2}\,|_{tol}\right)^{1.5}} \tag{A11}$$

In equation (A11), the *Skw_denom_coef* is used to reduce the skewness of vertical velocity that will be too large in the early hours of marine stratocumulus when *Skw* is large [*Bogenschutz et al.*, 2013]. $\tau_{max}$ represents


© 2014. The Authors.

AGU Journal of Advances in Modeling Earth Systems 10.1002/2014MS000315

the maximum of allowed time scale of $\tau$. *Lscale_pert_coef* is coefficient to perturb $\overline{\theta}_l$ and $\overline{q}_t$ for diagnosing eddy mixing length. $\mu$ and *Lscale_* $\mu$*_coef* perturb the fractional entrainment rate per unit altitude for calculation of eddy mixing length.

**Acknowledgments**
This study was supported by the U.S. Department of Energy's Office of Science as part of the Scientific Discoveries through Advanced Computing Program. The Pacific Northwest National Laboratory is operated for DOE by Battelle Memorial Institute under contract DE-AC05–76RL01830. V. Larson gratefully acknowledges support from the Office of Science (BER), U.S. Department of Energy, Grant DE-SC0008323. This research used resources of the National Energy Research Scientific Computing Center, which is supported by the Office of Science of the U.S. Department of Energy under Contract No. DE-AC02–05CH11231. All SCAM5 results are stored on a local PNNL cluster and are available upon request.

AQ7

## References

Abdul-Razzak, H., and S. J. Ghan (2000), A parameterization of aerosol activation: 2. Multiple aerosol types, *J. Geophys. Res.*, *105*, 6837–6844.
~~Ackerman, A. S., et al. (2009), Large-eddy simulations of a drizzling, stratocumulus-topped marine boundary layer, *Mon. Weather Rev.*, *137*, 1083–1110.~~ AQ8
André, J. C., G. De Moor, P. Lacarrere, and R. Du Vachat (1978), Modeling the 24-hour evolution of the mean and turbulent structures of the planetary boundary layer, *J. Atmos. Sci.*, *35*(10), 1861–1883.
Arakawa, A. (2004), The cumulus parameterization problem: Past, present, and future, *J. Clim.*, *17*, 2493–2525.
Bogenschutz, P. A., A. Gettelman, H. Morrison, V. E. Larson, D. P. Schanen, N. R. Meyrer, and C. Craig (2012), Unified parameterization of the planetary boundary layer and shallow convection with a higher-order turbulence closure in the Community Atmosphere Model: Single-column experiments, *Geosci. Model Dev.*, *5*(6), 1407–1423, doi:10.5194/gmd-5–1407-2012.
Bogenschutz, P. A., A. Gettelman, H. Morrison, V. E. Larson, C. Craig, and D. P. Schanen (2013), Higher-order turbulence closure and its impact on climate simulations in the Community Atmosphere Model, *J. Clim.*, *26*, 9655–9676, doi:10.1175/JCLI-D-13–00075.1.
Bony, S., and J. L. Dufresne (2005), Marine boundary layer clouds at the heart of tropical cloud feedback uncertainties in climate model, *Geophys. Res. Lett.*, *32*, L20806, doi:10.1029/2005GL023851.
Bougeault, P. (1981), Modeling the trade-wind cumulus boundary layer. Part I: Testing the ensemble cloud relations against numerical data, *J. Atmos. Sci.*, *38*, 2414–2428.
Bretherton, C. S., and S. Park (2009), A new moist turbulence parameterization in the Community Atmosphere Model, *J. Clim.*, *22*, 3422–3448.
Caflisch, R.E. (1998), Monte Carlo and quasi-Monte Carlo methods, *Acta Numer.*, *7*, 1–49.
Cheng, Y., V. M. Canuto, and A. M. Howard (2005), Nonlocal convective PBL model based on new third-and fourth-order moments, *J. Atmos. Sci.*, *62*(7), 2189–2204.
~~Duynkerke, P. G., and A. G. M. Driedonks (1987), A model for the turbulent structure of the stratocumulus-topped atmospheric boundary layer, *J. Atmos. Sci.*, *44*, 43–64.~~
Gaspar, P., Y. Grégoris, and J. M. Lefevre (1990), A simple eddy kinetic energy model for simulations of the oceanic vertical mixing: Tests at station Papa and Long-Term Upper Ocean Study site, *J. Geophys. Res.*, *95*(C9), 16,179–16,193.
Gettelman, A., H. Morrison, and S. J. Ghan (2008), A new two-moment bulk stratiform cloud microphysics scheme in the Community Atmosphere Model, version 3 (CAM3). Part II: Single-column and global results, *J. Clim.*, *21*, 3660–3679, doi:10.1175/2008JCLI2116.1.
Gettelman, A., X. Liu, S. J. Ghan, H. Morrison, S. Park, A. J. Conley, S. A. Klein, J. Boyle, D. L. Mitchell, and J.-L. F. Li (2010), Global simulations of ice nucleation and ice supersaturation with an improved cloud scheme in the Community Atmosphere Model, *J. Geophys. Res.*, *115*, D18216, doi:10.1029/2009JD013797.
Golaz, J.-C., V. E. Larson, and W. R. Cotton (2002a), A PDF-based model for boundary layer clouds. Part I: Method and model description, *J. Atmos. Sci.*, *59*(24), 3540–3551.
Golaz, J.-C., V. E. Larson, and W. R. Cotton (2002b), A PDF-based model for boundary layer clouds. Part II: Model results, *J. Atmos. Sci.*, *59*(24), 3552–3571.
Golaz, J.-C., S. Wang, J. D. Doyle, and J. M. Schmidt (2005), Model evaluation and analysis of second and third moment vertical velocity budgets, *Boundary Layer Meteorol.*, *116*, 487–517.
Golaz, J.-C., V. E. Larson, J. A. Hansen, D. P. Schanen, and B. M. Griffin (2007), Elucidating model inadequacies in a cloud parameterization by use of an ensemble-based calibration framework, *Mon. Weather Rev.*, *135*(12), 4077–4096, doi:10.1175/2007MWR2008.1.
~~Golaz, J.-C., M. Salzmann, L. J. Donner, L. W. Horowitz, Y. Ming, and M. Zhao (2011), Sensitivity of the aerosol indirect effect to subgrid variability in the cloud parameterization of the GFDL Atmosphere General Circulation Model AM3, *J. Clim.*, *24*, 3145–3160, doi:10.1175/2010JCLI3945.1.~~
Guo, H., J.-C. Golaz, L. J. Donner, V. E. Larson, D. P. Schanen, and B. M. Griffin (2010), Multi-variate probability density functions with dynamics for cloud droplet activation in large-scale models: Single column tests, *Geosci. Model Dev.*, *3*, 475–486, doi:10.5194/gmd-3–475-2010.
Guo, H., J.-C. Golaz, and L. J. Donner (2011), Aerosol effects on stratocumulus water paths in a PDF-based parameterization. *Geophys. Res. Lett.*, *38*, L17808, doi:10.1029/2011GL048611.
Guo, H., ~~J.~~-Golaz, L. J. Donner, P. Ginoux, and R. S. Hemler (2014), Multivariate probability density functions with dynamics in the GFDL atmospheric general circulation model: Global tests, *J. Clim.*, *27*, 2087–2108.
Hou, Z., M. Huang, L. R. Leung, G. Lin, and D. M. Ricciuto (2012), Sensitivity of surface flux simulations to hydrologic parameters based on an uncertainty quantification framework applied to the Community Land Model, *J. Geophys. Res.*, *117*, D15108, doi:10.1029/2012JD017521.
Lappen, C.-L., and D. A. Randall (2001), Toward a unified parameterization of the boundary layer and moist convection. Part I: A new type of mass-flux model, *J. Atmos. Sci.*, *58*, 2021–2036.
Larson, V. E., and J.-C. Golaz (2005), Using probability density functions to derive consistent closure relationships among higher-order moments, *Mon. Weather Rev.*, *133*(4), 1023–1042.
~~Larson, V. E., R. Wood, P. R. Field, J. C. Golaz, T. H. Vonder Haar, and W. R. Cotton (2001a), Small-scale and mesoscale variability of scalars in cloudy boundary layers: One-dimensional probability density function, *J. Atmos. Sci.*, *58*, 1978–1994.~~
~~Larson, V. E., R. Wood, P. R. Field, J. C. Golaz, T. H. Vonder Haar, and W. R. Cotton (2001b), Systematic biases in the microphysics and thermodynamics of numerical models that ignore subgrid-scale variability, *J. Atmos. Sci.*, *58*(9), 1117–1128.~~
Larson, V. E., J.-C. Golaz, and W. R. Cotton (2002), Small-scale and mesoscale variability in cloudy boundary layers: Joint probability density functions, *J. Atmos. Sci.*, *59*(24), 3519–3539.
~~Larson, V. E., J. C. Golaz, H. Jiang, and W. R. Cotton (2005), Supplying local microphysics parameterizations with information about subgrid variability: Latin Hypercube sampling, *J. Atmos. Sci.*, *62*, 4010–4026.~~
Larson, V. E., D. P. Schane, M. Wang, M. Ovchinnikov, and S. Ghan (2012), PDF Parameterization of Boundary Layer Clouds in Models with Horizontal Grid Spacings from 2 to 16 km, *Mon. Weather Rev.*, *140*, 285–306.
Liu, X., J. E. Penner, S. J. Ghan, and M. Wang (2007), Inclusion of ice microphysics in the NCAR Community Atmosphere Model version 3 (CAM3), *J. Clim.*, *20*, 4526–4547.

 © 2014. The Authors. 

AGU Journal of Advances in Modeling Earth Systems 10.1002/2014MS000315

~~Ma, P. L., P. J. Rasch, H. Wang, K. Zhang, R. C. Easter, S. Tilmes, J. D. Fast, X. Liu, J. H. Yoon, and J. F. Lamarque (2013), The role of circulation features on black carbon transport into the Arctic in the Community Atmosphere Model Version 5 (CAM5), *J. Geophys. Res.*, *118*, 4657–4669, doi:10.1002/jgrd.504.~~

McCullagh, P., and J. A. Nelder (1989), *Generalized Linear Models*, Chapman and Hall. AQ9

Moeng, C.-H., and R. Rotunno (1990), Vertical-velocity skewness in the buoyancy-driven boundary layer, *J. Atmos. Sci.*, *47*, 1149–1162.

Morrison, H., and A. Gettelman (2008), A new two-moment bulk stratiform cloud microphysics scheme in the Community Atmosphere Model, Version 3 (CAM3). Part I: Description and numerical tests, *J. Clim.*, *21*, 3642–3659, doi:10.1175/2008JCLI2105.1.

Park, S., and C. S. Bretherton (2009), The University of Washington shallow convection and moist turbulence schemes and their impact on climate simulations with the Community Atmosphere Model, *J. Clim.*, *22*, 3449–3469, doi:10.1175/2008JCLI2557.1.

Saltelli, A., and P. Annonia (2010), How to avoid a perfunctory sensitivity analysis, *Environ. Modell. Softw.*, *25*, 1508–1517.

Yang, B., Y. Qian, G. Lin, L. Y. R. Leung, and Y. Zhang (2012), Some issues in uncertainty quantification and parameter tuning: A case study of convective parameterization scheme in the WRF Regional Climate Model, *Atmos. Chem. Phys.*, *12*(5), 2409–2427, doi:10.5194/acp-12–2409-2012.

Yang, B., et al. (2013), Uncertainty quantification and parameter tuning in the CAM5 Zhang-McFarlane convection scheme and impact of improved convection on the global circulation and climate, *J. Geophys. Res.*, *118*, 395–415, doi:10.1029/2012JD018213, 2013.

Zhao, C., et al. (2013), A sensitivity study of radiative fluxes at the top of atmosphere to cloud-microphysics and aerosol parameters in the Community Atmosphere Model CAM5, *Atmos. Chem. Phys.*, *13*, 10,969–10,987, doi:10.5194/acp-13–10969-2013.

Author Proof

 © 2014. The Authors. 

AQ1 Please note that the reference Guo et al. [2013] has been changed to Guo et al. [2014] per the reference list.

AQ2 Please note that the citation of the reference Golaz et al. [2002] has been changed to Golaz et al. [2002a, 2002b]. OK?

AQ3 Please list the following references: Siebesma et al. [2003], Rauber et al. [2003], Stevens et al. [2005], Taylor [2001], Golaz and Larson [2001], and Rotta [1951] or delete the citations.

AQ4 Please note that Appendix B is cited but the same is not provided. Please provide the same.

AQ5 Please note that the reference McCullagh and Nelder [1998] has been changed to McCullagh and Nelder [1989] per the reference list. OK?

AQ6 Please confirm the insertion of equation number (A9) given to the equation is OK.

AQ7 Please check whether the edit made in the sentence "This study was supported by the U.S. Department of …" is OK.

AQ8 Please cite the references Ackerman et al. [2009], Duynkerke and Driedonks [1987], Golaz et al. [2011], and Larson et al. [2001a, 2001b, 2005] or delete from the reference list.

AQ9 Please provide the publisher location for the reference McCullagh and Nelder [1989].

706

Author Proof

WILEY-BLACKWELL

# USING e-ANNOTATION TOOLS FOR ELECTRONIC PROOF CORRECTION

**Required software to e-Annotate PDFs: Adobe Acrobat Professional or Adobe Reader (version 8.0 or above). (Note that this document uses screenshots from Adobe Reader X)**
**The latest version of Acrobat Reader can be downloaded for free at: http://get.adobe.com/reader/**

Once you have Acrobat Reader open on your computer, click on the Comment tab at the right of the toolbar:

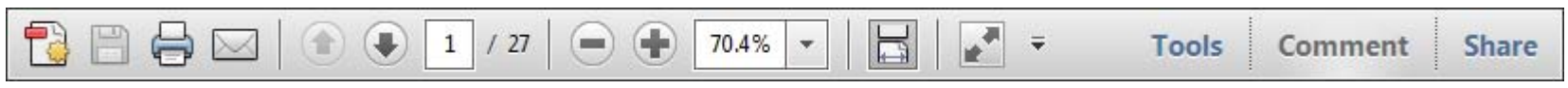


This will open up a panel down the right side of the document. The majority of tools you will use for annotating your proof will be in the Annotations section, pictured opposite. We've picked out some of these tools below:

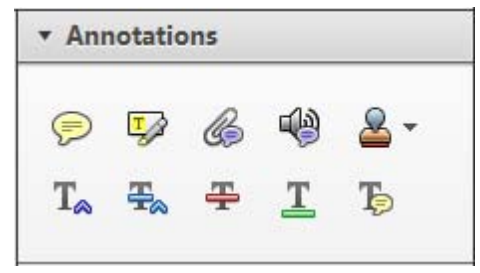


## 1. Replace (Ins) Tool – for replacing text.

Strikes a line through text and opens up a text box where replacement text can be entered.

**How to use it**

- Highlight a word or sentence.
- Click on the Replace (Ins) icon in the Annotations section.
- Type the replacement text into the blue box that appears.

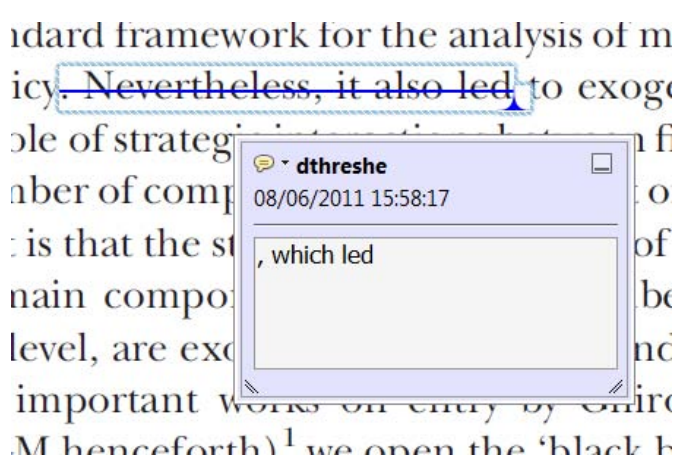


## 2. Strikethrough (Del) Tool – for deleting text.

Strikes a red line through text that is to be deleted.

**How to use it**

- Highlight a word or sentence.
- Click on the Strikethrough (Del) icon in the Annotations section.

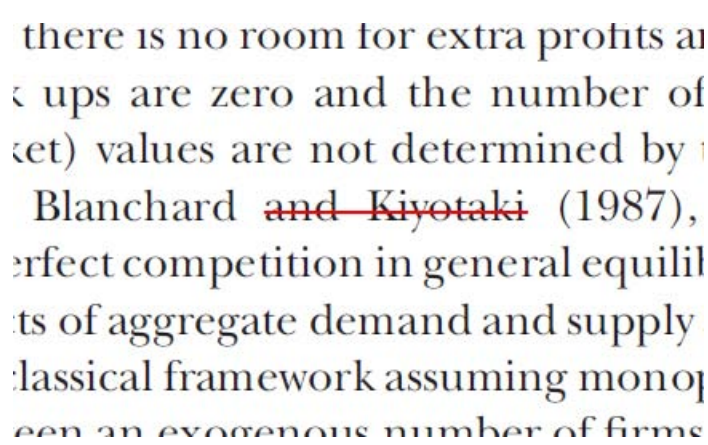

## 3. Add note to text Tool – for highlighting a section to be changed to bold or italic.

Highlights text in yellow and opens up a text box where comments can be entered.

**How to use it**

- Highlight the relevant section of text.
- Click on the Add note to text icon in the Annotations section.
- Type instruction on what should be changed regarding the text into the yellow box that appears.

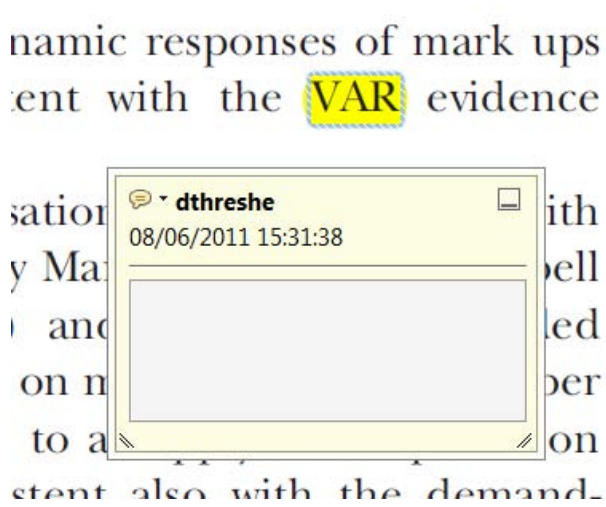


## 4. Add sticky note Tool – for making notes at specific points in the text.

Marks a point in the proof where a comment needs to be highlighted.

**How to use it**

- Click on the Add sticky note icon in the Annotations section.
- Click at the point in the proof where the comment should be inserted.
- Type the comment into the yellow box that appears.

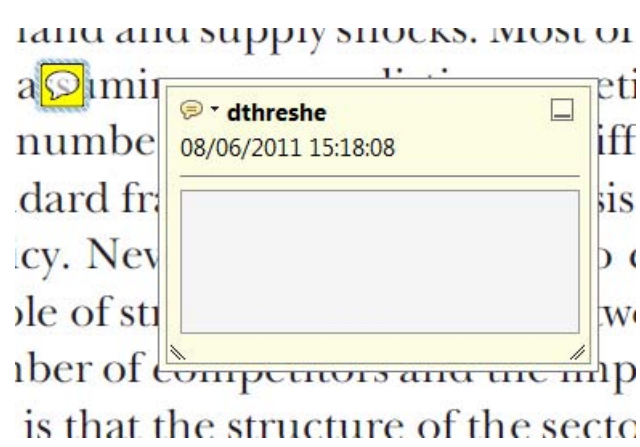

## USING e-ANNOTATION TOOLS FOR ELECTRONIC PROOF CORRECTION

### 5. Attach File Tool – for inserting large amounts of text or replacement figures.

Inserts an icon linking to the attached file in the appropriate pace in the text.

**How to use it**

- Click on the Attach File icon in the Annotations section.
- Click on the proof to where you'd like the attached file to be linked.
- Select the file to be attached from your computer or network.
- Select the colour and type of icon that will appear in the proof. Click OK.

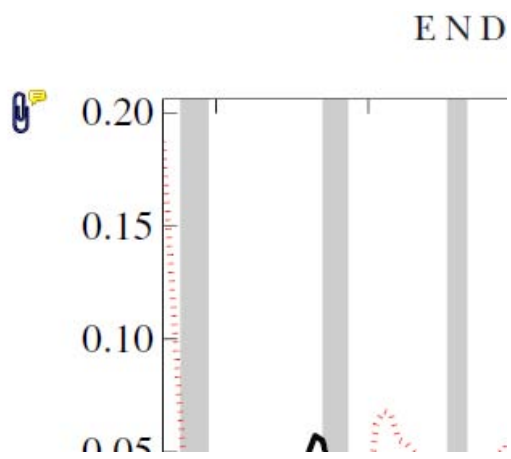


### 6. Add stamp Tool – for approving a proof if no corrections are required.

Inserts a selected stamp onto an appropriate place in the proof.

**How to use it**

- Click on the Add stamp icon in the Annotations section.
- Select the stamp you want to use. (The Approved stamp is usually available directly in the menu that appears).
- Click on the proof where you'd like the stamp to appear. (Where a proof is to be approved as it is, this would normally be on the first page).

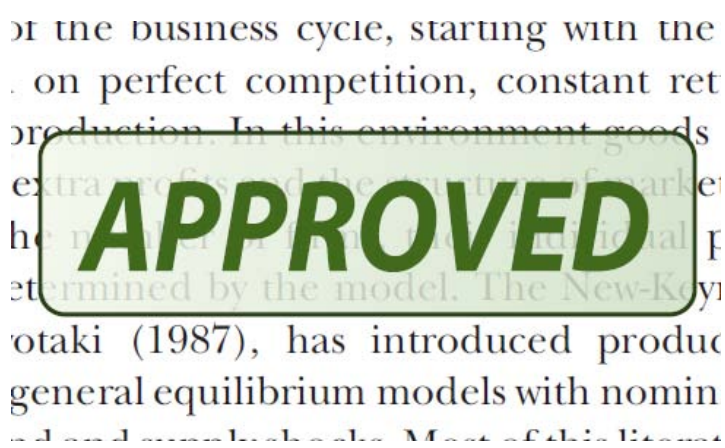


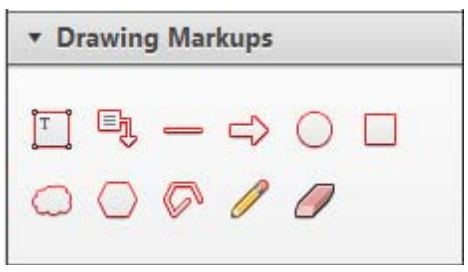


### 7. Drawing Markups Tools – for drawing shapes, lines and freeform annotations on proofs and commenting on these marks.

Allows shapes, lines and freeform annotations to be drawn on proofs and for comment to be made on these marks..

**How to use it**

- Click on one of the shapes in the Drawing Markups section.
- Click on the proof at the relevant point and draw the selected shape with the cursor.
- To add a comment to the drawn shape, move the cursor over the shape until an arrowhead appears.
- Double click on the shape and type any text in the red box that appears.

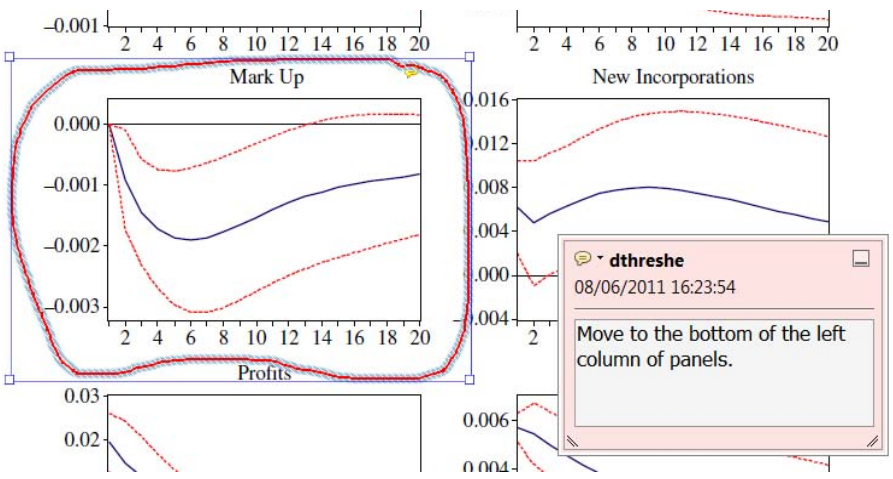


**For further information on how to annotate proofs, click on the Help menu to reveal a list of further options:**

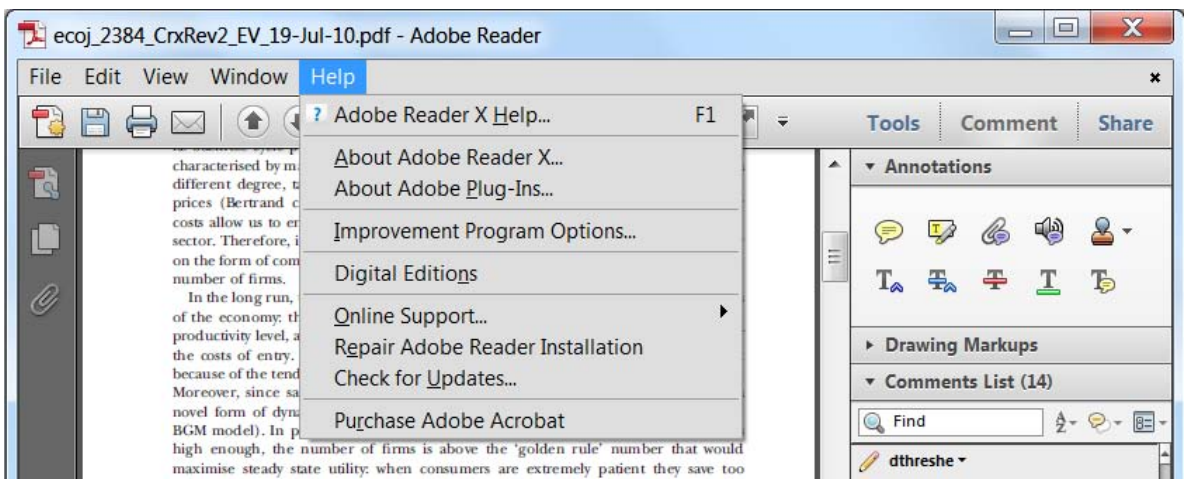

WILEY-BLACKWELL

**Additional reprint and journal issue purchases**

Should you wish to purchase additional copies of your article, please click on the link and follow the instructions provided: https://caesar.sheridan.com/reprints/redir.php?pub=10089&acro=JAME

Corresponding authors are invited to inform their co-authors of the reprint options available.

Please note that regardless of the form in which they are acquired, reprints should not be resold, nor further disseminated in electronic form, nor deployed in part or in whole in any marketing, promotional or educational contexts without authorization from Wiley. Permissions requests should be directed to mailto: permissionsus@wiley.com

For information about 'Pay-Per-View and Article Select' click on the following link: http://wileyonlinelibrary.com/ppv